Fluid Dynamics Analysis of Desktop-based Fused Deposition Modeling Rapid Prototyping

Mark Roxas
Stephen Ju

A thesis submitted in partial fulfilment
Of the requirements for the degree of

BACHELOR OF APPLIED SCIENCE

Supervisor: P.E. Sullivan

Department of Mechanical and Industrial Engineering
University of Toronto

March, 2008

Abstract

Recent improvements in the area of Fused Deposition Modelling have led to the creation of inexpensive desktop based Rapid Prototypers such as the Replicating Rapid-Prototyper (RepRap) allowing the individual the freedom to fabricate three dimensional parts of their own, however print resolutions of the parts are not on the same level as commercially based systems. It has been observed that adjusting the certain parameters on the polymer melt extruder such as the extruder nozzle diameter, nozzle angle, and liquefier length ultimately affects the extruded melt flow behaviour [17]. These parameters are important factors to consider for an improved design. This thesis presents the results of the computational and experimental work that shows the effect of taking the original specifications of the RepRap extruder and aims to show how reducing nozzle exit diameter and varying nozzle angle has resulting effects on the pressure drop and the flow behaviour of the melt. The results show that optimization of the flow rate can have significant effects on the extruded melt and it also shows limitations on how small the nozzle exit diameter can be before the resulting pressure drop becomes too large such that the motor cannot provide enough torque to drive the flow.

Ultimately, the proposed redesign suggests that the RepRap's extruder nozzle diameter can be decreased from 0.5mm to 0.3mm with a nozzle angle of 120 degrees which will decrease the diameter of the extruded melt contributing to better resolutions. The report further shows the consequences of further decreasing the diameter and nozzle angle and concludes with an experiment that observes the melt flow behaviour of the melt to ensure that PCL is a valid candidate material for Fused Deposition Modelling in Rapid Prototyping.

Acknowledgements

There are several people who have to be acknowledged for the completion of this thesis project. Most importantly, many thanks go to Professor P.E. Sullivan for being our supervisor and even more for providing us with support and guidance in undertaking our thesis project.

We would also like to thank Dr. Adrian Bowyer, Ian Adkins and contributing members of the RepRap Research Foundation for providing an open-source rapid prototyping project for us to study, as well as providing comments and suggestions supporting our project.

Table of Contents

List of Symbols

Symbol	Definition
L_1, L_2 and L_3	Length of geometric zones of the liquefier
β	Nozzle Angle
$\emptyset$	Fluidity constant that characterizes ability of material to flow
m	Flow exponent - Material index that measures of how the material flow characteristics deviate from Newtonian flow
V_1	Entrance velocity
T	Working temperature (or flow channel temperature). This temperature must be maintained slightly above the PCL melting temperature to allow quicker cooling to prevent fluid deformation
$T_\propto$	Temperature at which $\emptyset$ and m are calculated
T_o	Absolute temperature
σ	Activation Energy
d	Nozzle exit diameter
α	Nozzle angle
ΔP	Pressure Drop
$\bar{v}$	Mean Velocity
r	Radius
η	Viscosity
T	Torque
F	Force
ω	Angular Velocity
τ	Shear Stress
T_d	Drive Torque
V	Voltage
I	Current
d	Mean filament diameter at liquefier exit
d_s	Mean filament diameter after solidification

List of Figures

List of Tables

1.0 Introduction

The intent of this study was to improve the current design of an extruder liquefier (one component of the extruder) used in a desktop rapid prototyping technology called the Replicating Rapid Prototyper (RepRap). The main focus was on how to improve the extruder head rather than the system as a whole. A computational fluid dynamics approach was used to study the relationship between the internal flow geometry of the extruder and the melt flow behaviour of a non-Newtonian fluid called Polycaprolactone (PCL) used for this application. Two key parameters: *Pressure Drop* across the liquefier and *Nozzle Exit Diameter*, are tuned to enhance the *Print Resolution*.

Rapid Prototyping is a layered manufacturing technique that prints a three dimensional physical object created from a virtual model in computer-aided design modeling software. The various types of rapid-prototyping technologies may be classified by the methods used in their solid freeform fabrication technique [9]. Some common technologies are Stereolithography (SLA), Fused-Deposition Modelling (FDM), and Selective Laser Sintering (SLS) [15]. Each of these technologies use different tool heads, operate at different temperatures, and use different deposition materials.

Rapid Prototyping technologies (RPT) currently exists in the market as large and expensive commercial systems available only to institutions that can afford them. The potential direction of Rapid Prototyping is toward creating desktop-based solutions that provide equivalent functionality and performance of a commercial system at a cost low enough, to make it accessible to the general public. Public interest would be served by having a desktop manufacturing device at home that could produce quality 3D parts. Having this technology would no longer limit product design to large corporations but open it up to creative individuals.

There are currently two desktop-based Rapid Prototypers widely known in the Rapid Prototyping community and these are Fab@home [11] and Replicating Rapid-Prototyper (RepRap) [4] projects, and their variants, both of which provide a cheaper alternative to the commercial systems that currently exist. Both systems use the FDM technique and therefore this technique will be the focus of this thesis.

The main objective of this thesis is to generate an improved design of a current desktop rapid-prototyping technology, namely, the Replicating Rapid-Prototyper (RepRap), shown in Figure 1.

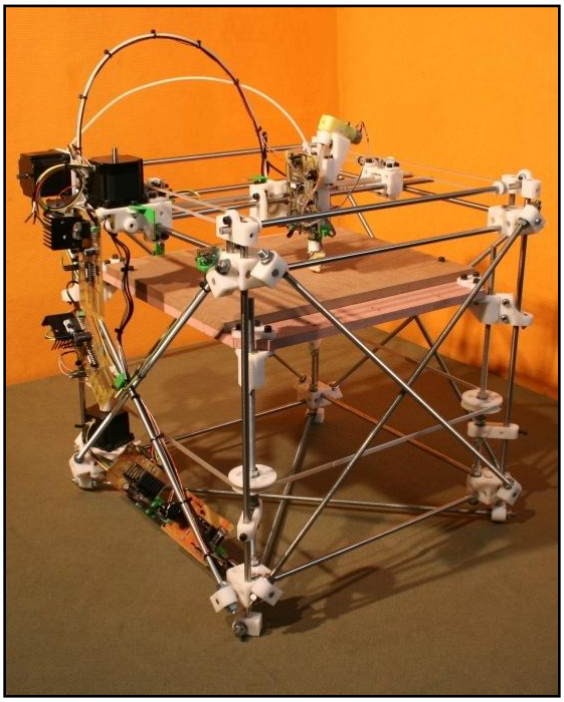

Figure 1 Replicating Rapid Prototyper (RepRap)
(Image taken taken from www.reprap.org)

A thorough examination of the RepRap's plastics extruder / material deposition tool will be undertaken to determine whether the design can be improved with respect to the *Print Resolution*. This will be done through carrying out an analysis of the melt flow behaviour of PCL

via computational modeling, mathematical modeling, as well as a laboratory experiment that will characterize the flow.

2.0 Methodology

This research takes a fluid dynamics approach to improve the print quality or *Print Resolution* of the RepRap. This will be achieved through analyzing the extruder subassembly (Figure 2). The print material is Polycaprolactone (PCL), as it is the currently preferred FDM thermopolymer for the RepRap [4]. The cylindrical rod section near the end of the extruder is called the liquefier (Figure 3 and Figure 4), which is connected to heating elements that melt the polymer prior to extrusion. It should be clarified that the liquefier is made of brass, and is coated in a layer of PTFE tape as an insulator to prevent heat loss. The brass liquefier is actually the central area of focus since its internal geometry serves as the flow channel for the PCL melt. Polycaprolactone's performance was analyzed using the Floworks CFD software and experimental methods.

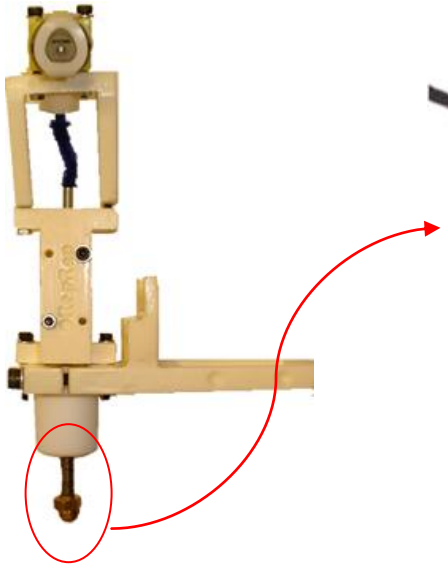

Figure 2 RepRap Extruder

Figure 3 Liquefier Section

(Image taken from www.reprap.org)

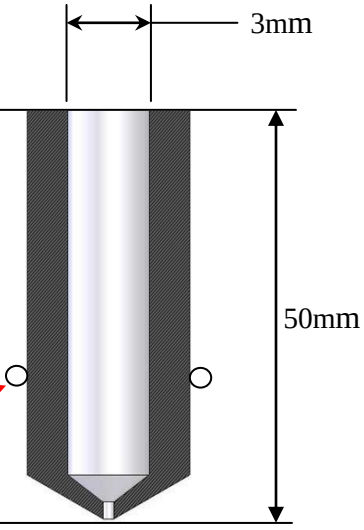

Figure 4 Internal Flow Geometry of liquefier

To clarify, the *Print Resolution* of the RepRap refers to the thickness and consistency of the PCL extrudate upon exit. It is a critical parameter that constitutes the performance of the RepRap, and is governed directly by the following three variables:

1. *Temperature of melt flow*. It is important not to overheat the PCL melt to an excessively high temperature because the fluidity will increase, which in turn will cause excessive filament elongation and inconsistent filament diameter upon exit. This degrades the surface finish of the printed part.
2. *Pressure drop (ΔP).* The pressure drop directly affects the amount of force required to push the filament through. Controlling the amount of force applied to the filament will prevent any build up of material melt within the liquefier which can cause a feedback effect, further increasing the pressure drop. Controlling the force can keep the exit extruded melt as a consistent stream with non-varying thicknesses. Any changes in layer thickness can contribute to overall part defects.
3. *Nozzle exit diameter (d).* In order to maintain a fine filament diameter, the nozzle exit diameter needs to be a small as possible.

The *Temperature of melt flow* can be modified to improve the *Print Resolution* simply by modifying the boundary conditions. This will be demonstrated in chapter 3.0 of this paper. However, *Pressure drop* and *Nozzle exit diameter* are more complicated to tune. This is because *Print Resolution* is a function of both the *Nozzle exit diameter* and the *Pressure drop (ΔP)*. These relations are illustrated in Figure 5.

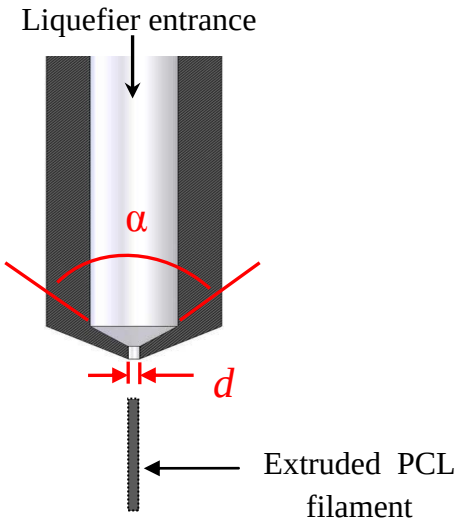

Smaller the better

$$Print\ Resolution = f(T, \Delta P, d)$$

$$\Delta P = f(\alpha, d)$$

Figure 5 Brass Rod Liquefier Design Variables

Thus a problem arises where reducing the value of *d* excessively may compromise the overall *Print Resolution* instead of improving it. For example, if *d* is proportional to *Print Resolution* and inversely proportional to *ΔP*, a methodology for optimizing the *Print Resolution* is needed. The effect of the *Nozzle exit diameter (d)* on the *Print Resolution* is illustrated in chapter 3.2.1. Note: the two relations represented in Figure 5 is explained by means of theoretical and numerical studies in chapter 3.2. The variables *d* and *α* are of particular interest, and will receive the most attention in this study. Some principles of Design of Experiments were considered to examine the *Pressure Drop (ΔP)* across the liquefier as a function of *Nozzle angle (α)* and *Nozzle exit diameter (d)* by:

- Varying the nozzle diameter, *d* (Note: original *d* = 0.5mm)
- Varying the nozzle angle, α (Note: original α = 120^o)

Since Polycaprolactone (PCL) is a Pseudoplastic (shear thinning) fluid, the viscosity decreases with increasing shear rate, which also decreases the Reynold's number below 1, classifying this

flow as creeping flow. Therefore, viscous forces dominate inertial forces at this small scale, and was expected that there would be a change in pressure drop by varying nozzle parameters mentioned above. A total of sixteen cases were investigated using Floworks, and a graph of nozzle angle versus pressure drop was constructed for the CFD model. This is shown in chapter 3.2. Quantitatively speaking, the best combination of *d* and α is one that results in the least pressure drop, ΔP. Smaller ΔP values mean that less compressive force is required by the drive screw to push the material feedstock through the extruder. The amount of force was translated to a torque needed from the drive screw motor. This was used to determine an appropriate motor RPM setting.

On the whole, the challenge was to procure an improved *Print Resolution* for the RepRap via modification of the three variables, with focus on *Pressure Drop (*ΔP).

2.1 Current Problems with the Original RepRap Machine

The original RepRap brass rod liquefier contains several problems that stem from the pre-defined boundary conditions of the internal flow channel. The PCL melt reaches its melting temperature (330K) at approximately 15mm from the inlet (see Appendix A1 for cross-reference). However, this temperature continued to rise to a maximum of about 413K (at the exit). This is not favourable because of the following:

a) *Deviation from isothermal assumption.* In our mathematical model, an isothermal condition across the length of the liquefier was assumed. Therefore, the more variation in temperature, the higher the deviation from the mathematical model.

b) *Poor Print Resolution*. Increasing the temperature above its melting temperature by such a high magnitude will ultimately increase the fluidity (ϕ) of PCL. It will be shown later in the mathematical model that $\mu \propto \frac{1}{\phi}$ where μ is the dynamic viscosity.

If μ is lowered, the extruded filament at nozzle exit will exhibit excessive strain and random behaviour. Thus the *Print Resolution* is compromised.

c) *Higher power demands for heating*. From Appendix A1, the excessive power input to heat the PCL is 83K above its melt flow temperature (330K) is unnecessary and wasteful, and should be reduced to improve efficiency.

d) *Slower solidification*. Since the PCL is heated to 413K, the rate at which the filament will cure or solidify is longer, which increases the total build time.

3.0 Improving Boundary Conditions for the Liquefier

3.1 Using the Mathematical Model

A theoretical model was developed as a basis for modeling the pressure drop across the liquefier.

The compressive force applied on the material filament has to overcome the pressure drop in the liquefier. This compressive force is applied through a screw which is driven by a motor. The relationship between the force, F and the torque, T in the motor is

$$T = \frac{F}{2} \cdot R$$

$$Power = T \cdot \omega$$

where *R* is the shaft radius and ω the angular velocity of the motor. The mathematical model is a relationship that describes the pressure drop across the liquefier. The derivation of which is covered in this section.

The liquefier is divided into three geometrical zones (see Figure 6) and each zone has a pressure drop equation for its particular geometry. The total pressure drop is the summation of the pressure drop across the three zones.

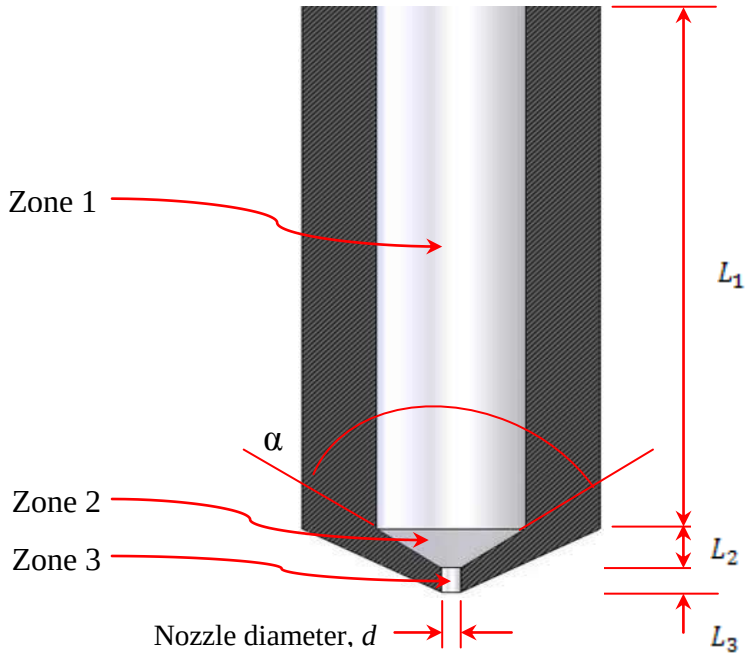

Figure 6 Mathematical Representation

There are a number of assumptions made to derive these equations [12]:

- Steady state flow: no transient change in the flow at any point in the flow channel
- Slow moving flow: the forces of inertia should be negligible when compared to the friction forces; the flow is to be laminar based on low Reynolds numbers.
- Isothermal flow: all particles of the fluid have the same temperature
- Hydrodynamically fully developed flow
- Incompressible fluid: the density is constant
- No external forces
- The effect of gravity is neglected
- The velocity of the fluid at the wall is 0 (no-slip boundary condition)

The derivation of the pressure drop across zone 1 (flow through a circular channel) is treated in this report with equations derived by Bellini [2].

Pressure drop across zone 1

The derivation begins by considering a momentum flux balance on a cylindrical differential fluid element with thickness *dr* and axial length *dz*, within a circular channel of radius R, and length L [12] (see Figure 7). Since the fluid flows on straight, parallel paths with uniform velocity and because of the assumption of an incompressible fluid, the momentum flux balance is simplified to a force balance.

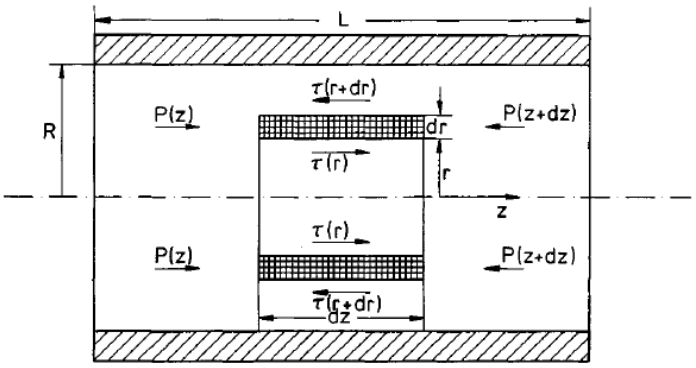

Figure 7 Force balance on the cylindrical fluid element (source: Michaeli [12])

$$2\pi r dr\,[p(z) - p(z+dz)]\; + \tau 2\pi r dz - \tau(r+dr)\cdot 2\pi\cdot(r+dr)dz = 0 \qquad (1)$$

By developing the Taylor Series up to the first term, subsequent substitution into the force balance reduces the equation to:

$$p(z+dz) = p(z) + \frac{\partial p}{\partial z}dz$$

$$\tau(r+dr) = \tau(r) + \frac{\partial \tau}{\partial r}dr$$

$$2\pi r\,dr\,\left[p(z) - p(z) - \frac{\partial p}{\partial z}dz\right]\; + \tau 2\pi r\,dz - \left(\tau + \frac{\partial \tau}{\partial r}dr\right)\cdot 2\pi\cdot(r+dr)dz = 0$$

Further simplification results in the expression:

$$-r\frac{\partial p}{\partial z} - \left(\tau + \frac{\partial \tau}{\partial r}r + \frac{\partial \tau}{\partial r}dr\right) = 0$$

Under the assumption of fully developed flow, the pressure gradient is a constant value related by the pressure drop across the cylinder and the total length.

$$\frac{\partial p}{\partial z} = \frac{\Delta P}{\mathrm{L}}$$

Substituting this relation into the expression and further simplification yields a differential equation:

$$-r\frac{\Delta P}{\mathrm{L}} - \left(\tau + \frac{\partial \tau}{\partial r}r + \frac{\partial \tau}{\partial r}dr\right) = 0$$

$$-r\frac{\Delta P}{\mathrm{L}} = \tau + \frac{\partial \tau}{\partial r}(r + dr)$$

$$\frac{\Delta P}{\mathrm{L}} = -\frac{\tau}{r} - \frac{\partial \tau}{\partial r}\left(\frac{r + dr}{r}\right) = -\frac{\tau}{r} + \frac{d\tau}{dr} + 2\,\frac{\tau}{r}$$

$$\frac{\Delta P}{\mathrm{L}} = \frac{\tau}{r} + \frac{d\tau}{dr}$$

The solution of the first order differential equation characterizes the shear stress in the zone 1 and it is

$$\tau = \frac{\Delta P}{2L}r + \frac{C}{r}$$

The constant C is found by applying the boundary condition that at r = 0, there are no shear forces, therefore, C =0 and the relationship now becomes

$$\tau = \frac{\Delta P}{2L}r$$

The above relation for shear stress does not consider the material behaviour. To account for material properties and the deviation of the flow behaviour from a Newtonian fluid we use the power law. The power law is expressed as:

$$\mu = K \cdot \dot{\gamma}^{n-1}$$

Where μ is the dynamic viscosity, K is the flow consistency index, and n is flow behaviour index. However, if the following substitutions are made:

$$n = \frac{1}{m}$$

$$K = \phi^{-\frac{1}{m}}$$

$$\mu = \phi^{-1} \cdot \tau^{1-m}$$

With ϕ representing the fluidity and m is the flow exponent. The resulting expression is known as the Power Law (Ostwald and de Waele [6,14]).

$$\tau = \left(\frac{1}{\phi}\right)^{\frac{1}{m}} \cdot \left(-\frac{dv}{dr}\right)^{\frac{1}{m}}$$

Substituting this form of the power law into expression equating the two shear stresses,

$$\frac{\Delta p}{2L} r = \left(\frac{1}{\phi}\right)^{\frac{1}{m}} \cdot \left(-\frac{dv}{dr}\right)^{\frac{1}{m}}$$

$$\dot{\gamma} = \frac{dv}{dr} = -\phi \left(\frac{\Delta P}{2L} r\right)^{m}$$

The integration of this equation yields a relationship to characterize the velocity of the fluid at position r:

$$v_2(r) = -\phi \left(\frac{\Delta P}{2L}\right)^{m} \int r^m \, dr = -\phi \left(\frac{\Delta P}{2L}\right)^{m} \frac{r^{m+1}}{m+1} + C$$

For $r = R \; and \; v_2 = 0$ corresponding to the 0-slip condition

$$C = \phi \left(\frac{\Delta P}{2L}\right)^{m} \frac{R^{m+1}}{m+1}$$

$$v_2(r) = \phi \left(\frac{\Delta P}{2L}\right)^{m} \frac{R^{m+1} - r^{m+1}}{m+1}$$

The mean velocity is expressed as

$$\bar{v} = \phi \left(\frac{\Delta P}{2L}\right)^m \frac{r_1^{m+1}}{m+3}$$

From which the final expression for pressure drop is obtained after re-arranging

$$\Delta P_1 = 2L \left(\frac{V}{\phi}\right)^{\frac{1}{m}} \left(\frac{m+3}{r_1^{m+1}}\right)^{\frac{1}{m}}$$

$$\eta = H(T) \cdot \eta_0(\dot{\gamma})$$

For Newtonian fluids, viscosity is related to temperature by an Arrhenius relation. Although the PCL melt is pseudo-plastic, its flow properties can be considered Newtonian at zero shear rates since thermal effects continually regenerate the entangled polymer chains [7]. Therefore, the Arrhenius type expression of the form:

$$H(T) = exp\left[\sigma\left(\frac{1}{T - T_0} - \frac{1}{T_\alpha - T_0}\right)\right]$$

is applicable. Where T_α is the reference temperature for which H(T) = 1 and $T_0 = 0$ for absolute temperatures. With the Arrhenius relation for temperature dependent viscosity, the expression for the pressure drop now becomes:

$$\Delta P_1 = 2L_1 \left(\frac{V}{\phi}\right)^{\frac{1}{m}} \left(\frac{m+3}{r_1^{m+1}}\right)^{\frac{1}{m}} exp\left[\sigma\left(\frac{1}{T - T_0} - \frac{1}{T_\alpha - T_0}\right)\right]$$

Similarly, the other two pressure drop equations ΔP_2 and ΔP_3 are for zones 2 and 3 can be derived by using the assumption of low Reynold's number flow and discretizing the conical zone into differential cylindrical zones and summating them. The derivations have been done by Bellini and the final expressions are presented as follows:

$$\Delta P_2 = \frac{2m}{3\tan\frac{\alpha}{2}} \left(\frac{1}{r_2^{\frac{3}{m}}} - \frac{1}{r_1^{\frac{3}{m}}}\right) \left(\frac{V}{\phi}\right)^{\frac{1}{m}} [r_1^2 2^{m+3}(m+3)]^{\frac{1}{m}} \cdot e^{\left[\sigma\left(\frac{1}{T-T_0} - \frac{1}{T_\alpha - T_0}\right)\right]}$$

$$\Delta P_3 = 2L_3 \left(\frac{V}{\phi}\right)^{\frac{1}{m}} \left(\frac{r_1^2(m+3)}{r_2^{m+3}}\right)^{\frac{1}{m}} \cdot e^{\left[\sigma\left(\frac{1}{T-T_0}-\frac{1}{T_\alpha-T_0}\right)\right]}$$

Note: explanations for each parameter in these pressure drop equations can be found in the list of symbols at the beginning of this report.

The total pressure drop would be:

$\Delta P = \Delta P_1 + \Delta P_2 + \Delta P_3$

ΔP_2 and ΔP_3 are of particular interest here because they depend on the cross sectional area, which can be easily modified by changing $\propto$ and d.

When the filament enters the brass rod liquefier (in its solid state), it acts as a piston to push the molten material toward the exit with an applied force, F. By knowing the total pressure drop, ΔP the applied force to compress the filament at the liquefier inlet can be calculated as:

$F = \Delta P \; x \; A$

The material flow behaviour deviates from the assumed steady state conditions where the flow profile does not change with time. ΔP does fluctuate over time. This could potentially compromise the quality of the filament upon exit by producing non-uniform filament width and result in poor surface finish upon solidification. Therefore, choosing the optimal power settings for the motorized drive wheels is integral to the print resolution.

There may be a direct correlation between pressure drops and the geometry of the flow channels [8], particularly near the exit. To test this hypothesis, the channel geometry was modified by:

- Varying the nozzle diameter, *d* (Note: original *d* = 0.5mm)
- Varying the nozzle angle, α (Note: original α = 120^o)

which is the exact same approach as represented in the CFD model. A total of sixteen cases were performed using the pressure drop equations; a graph of nozzle angle versus pressure drop was then constructed for the mathematical model in next section.

3.1.1 Mathematical Model Results

Using MATLAB, the pressure drop equations were solved for the current RepRap's specified nozzle dimensions (0.5mm diameter and 120 degrees nozzle angle) as well as three other nozzle diameters with varying nozzle angles. The results in Figure 8 show that pressure drop increases with decreasing nozzle diameter and nozzle angle. The data obtained from MATLAB was later compared with those of the numerical model.

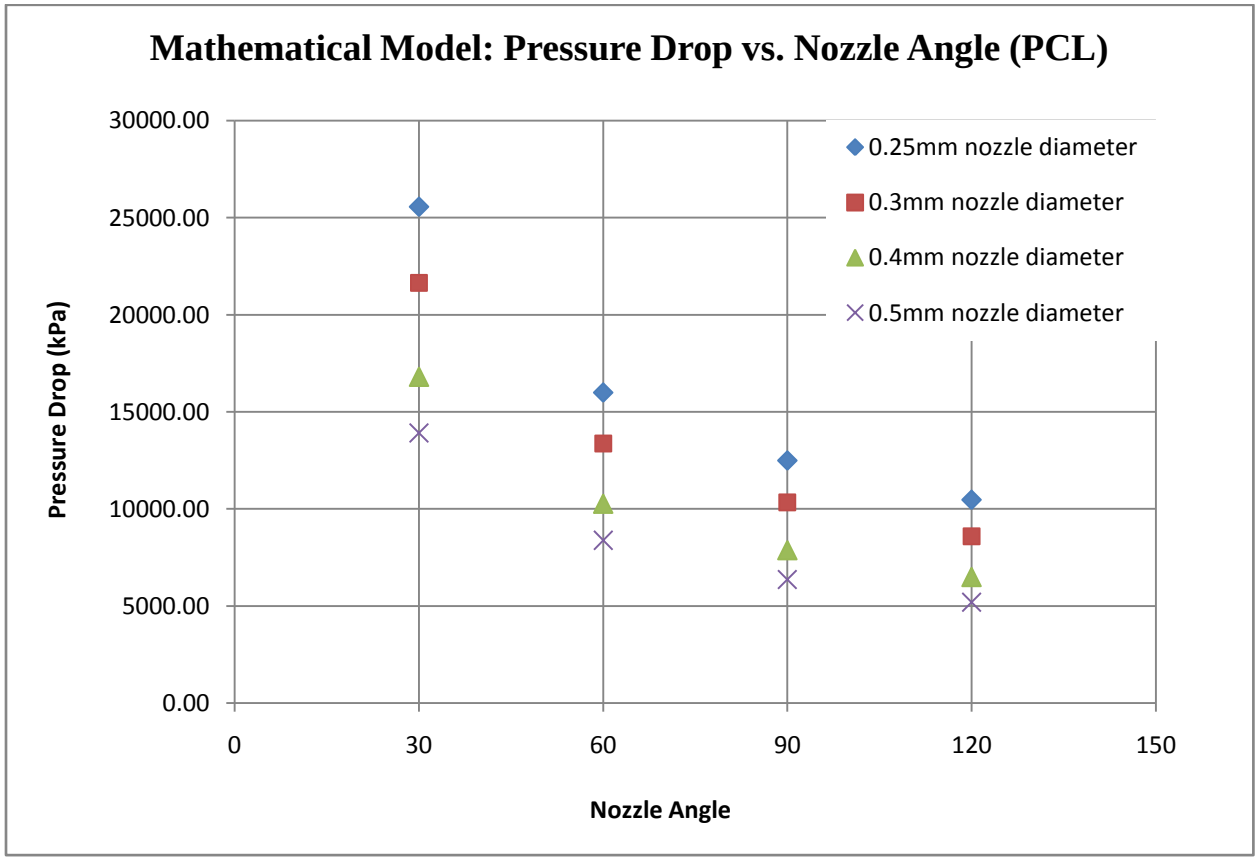

Figure 8 The Mathematical Model: Pressure Drop vs. Nozzle Angle (PCL)

3.1.2 Mathematical Model Sensitivity Analysis

To determine whether or not the theoretical model is valid, it was tested by studying how the variation in output changes with varying parameters in the equations.

The mathematical model is defined by three equations whose parameters contribute to the characterization of the pressure drop across the liquefier. The equations are composed of parameters related either to the geometry, fluid properties, or temperature.

Complete information regarding the geometry of the model has been provided and the processing temperatures of the fluid remain consistent in literature. However, since the fluid is Pseudoplastic there was uncertainties with regards to the fluid property terms. Therefore, to evaluate the confidence of the model, the model is tested by adjusting the material index and fluidity terms in the model and the output was observed to see how sensitive the model is to minor variations in these parameters. If the output was found to have large variations from the chosen indices then a closer examination of the chosen values needs to be taken into account.

Fluidity constant, φ

The consistency index of PCL changes with temperature [10]. Any variations in temperature can affect the fluidity constant. The model is tested by varying the fluidity constant to 10% and 20% from the source value.

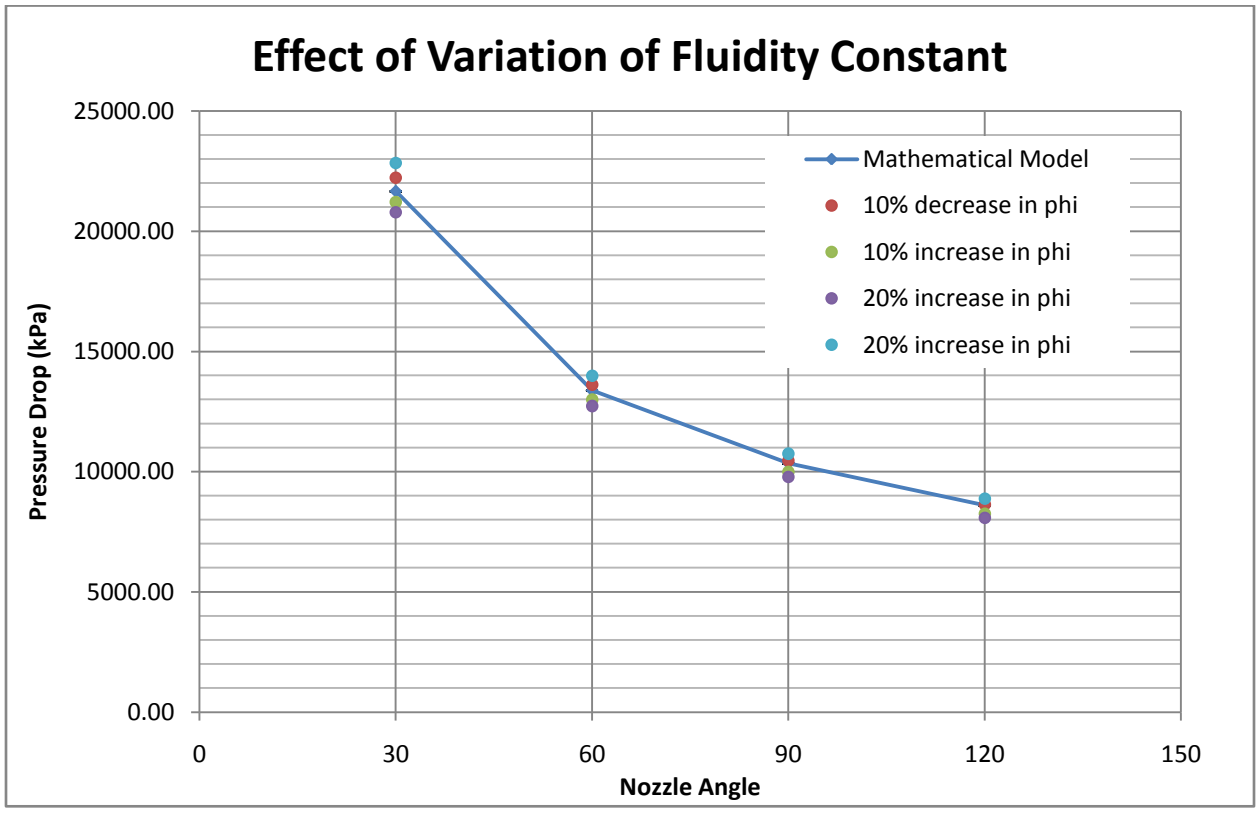

Figure 9 Effect of varying Fluidity Constant

Figure 9 shows the effect of varying the fluidity constant of the results of the mathematical model. The variation in the pressure drop at each nozzle angle is not severely affected by significant changes in the fluidity constant.

Material index, m

The material index is the exponent of the exponential curve relating viscosity to the shear rate. The power law curve for PCL changes with different temperatures, thereby significantly changing the material index, m. The typical range of m for PCL is 1.4 to 5 [18]. The best available data for the material index of PCL was taken at a temperature of 130°C which is a value of 4.29. The model is tested by varying the index from a lower bound of 20% of the original value to the upper bound of 5.

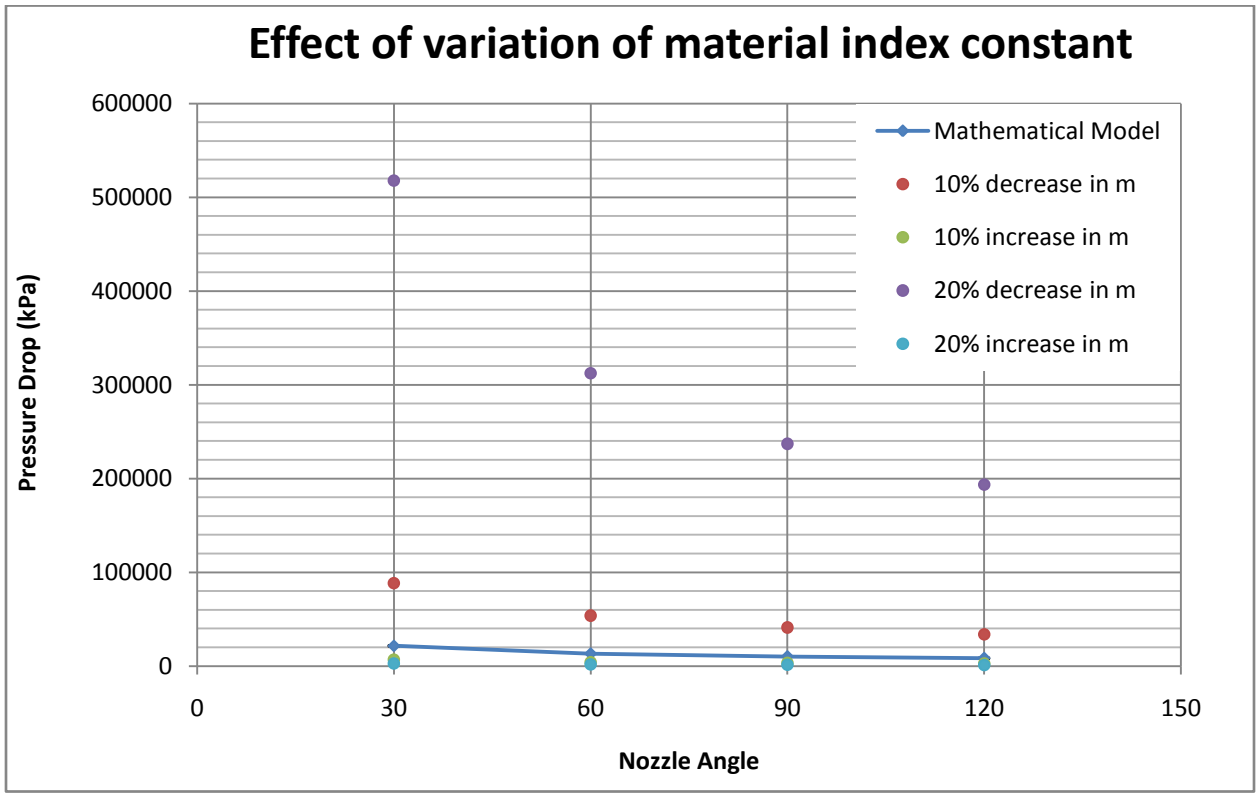

Figure 10 Effect of Variation of Material Index

Figure 10 shows that the model is extremely sensitive to changes in material index. By testing the lower bound, the pressure drop would increase by several orders of magnitude. Lower values of m appear to show a poor model due to high pressure drop values, the material index for PCL was taken at 130°C, at lower temperatures the value of m will increase. Therefore, at the melting temperature for PCL of approximately 62°C, it is certain that the index m, is in the range between 4.29 and 5. Figure 10 shows that for increasing m, the value of the pressure drop decreases but remains in the same order of magnitude. This range does not show a large variation in pressure drop so there is a reasonable amount of confidence in the model.

Uncertainties

The experimental data to determine the power law relationship for PCL was shown to be for shear rates greater than $100s^{-1}$. The shear rate for the scale of this project is on the order

between 1 and 10 s^{-1}. The power law model in the experimental data may not be an entirely accurate model to obtain a material index that does not contain data points for shear rate tests below $100s^{-1}$.

3.1.3 Mathematical Model Limitations

The results from the mathematical model are subject to certain error. The equations describing the pressure drop are sensitive to minor changes in the material index and flow consistency index for the particular material in consideration. The two indices were obtained through curve fitting using experimental data from external sources. Ideally, material and flow constants should be obtained by examining the material melt flowing through the RepRap's liquefier and measuring the viscosity through varying shear rate and finding the corresponding constants that fit experimental data. However, these experiments were never carried out. In general, the theoretical model takes into consideration many assumptions which idealize the melt flow behaviour. Some of these assumptions (e.g. steady state flow and isothermal conditions) are simplifications that do not necessarily model the actual behaviour. Combined with the sensitivity to the material index parameter, there are variations in the resulting pressure drop values. Therefore, the theoretical model alone is insufficient to portray pressure drop. The following chapter evaluates the validity of the theoretical model using numerical modeling (Computational Fluid Dynamics).

3.2 The Equivalent Numerical Analysis (CFD Model)

Bellini proposed a different set of boundary conditions during a similar experiment that examines the melt flow behaviour of PCL [2]. These conditions were shown to be more efficient compared to the current RepRap settings. Incorporating these findings to the RepRap liquefier, an improved model was implemented by using Floworks and shown in Appendix A2. These

new boundary conditions not only conserves power, but also allows PCL to reach its melt flow temperature of 330K at 17mm (only 2mm more than in the original scenario), and maintains a flow rate that allows the system to adhere to the isothermal assumption with greater confidence. This facilitates a more accurate comparison with the mathematical model. But most importantly, the exit diameter of the extruded filament will be more consistent than before because of the lower temperature and reduced fluidity.

The effects of *Nozzle exit diameter (d)* and *Nozzle angle (α)* on *Print Resolution* needed to be investigated. Increasing both α and d would decrease *Pressure drop (ΔP)* [2]. But since print quality is the critical parameter to be optimized, it was also necessary to decrease d (recalling that *Print Resolution* is a function of both pressure drop and nozzle diameter). But it is uncertain if decreasing d further will lead to any undesirable trade-offs such as an increase in ΔP, which in turn decreases the overall *Print Resolution* since ΔP grows with decreasing d. If indeed this is an undesirable trade-off, then to what extent should the nozzle diameter be reduced (if reduction is needed at all), in order to obtain the best overall α and d combination such that print resolution is optimized? These questions are answered. To begin, it is a safe approach to use this improved model as a baseline (i.e. with d=0.5mm, α=120^o), and incorporate additional incremental improvements by means of CFD.

3.2.1 Obtaining an Improved *d* and *α* Combination

The parameters d and α were selected on a quantitative and qualitative basis. Figure 11 shows a plot of ΔP vs. $\propto$ for four different values of d. Beginning with the baseline model (d=0.5mm, α=120^o), it was seen that changing the nozzle angle and nozzle diameter both have an impact on pressure drop. The CFD model simulated the flow of material under a variety of different nozzle angles and diameters and it was compared to the base case of 0.5mm nozzle

diameter with a 120 degree angle. The 0.25mm diameter case was chosen because many commercial FDM RPT systems extrude melts at that diameter [22] and therefore it was prudent to try and see if the RepRap can achieve the same resolution. However, at 0.25mm, the CFD analysis yielded enormous pressure drops.

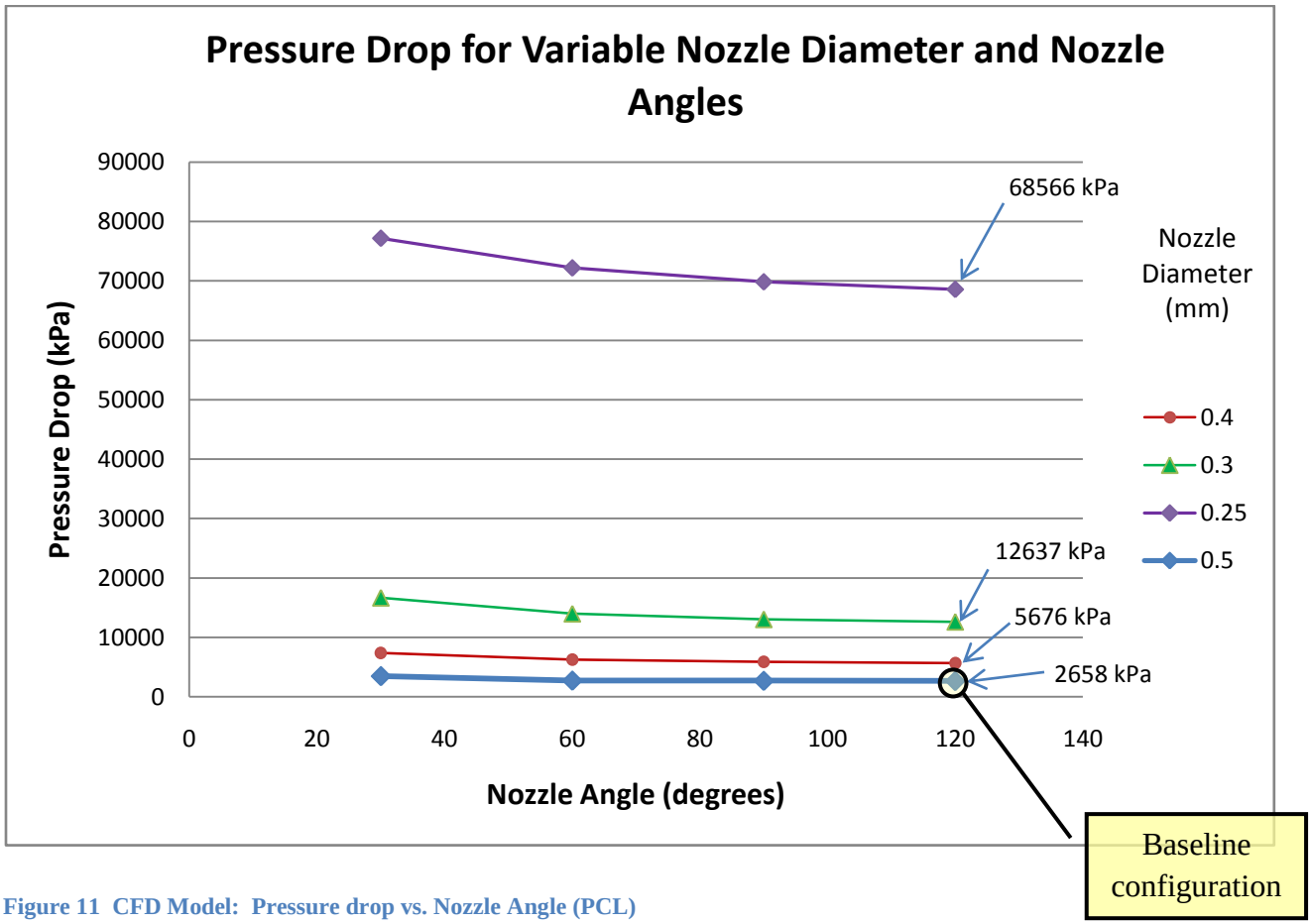

Figure 11 CFD Model: Pressure drop vs. Nozzle Angle (PCL)

Furthermore, it can be noted that the pressure drop was the lowest for α=120^{o} for all four nozzle diameters. Thus, it is clear that the higher the nozzle angle, the lower the pressure drop. This is important at the higher pressure drops. As for the nozzle diameter (d), the same reasoning cannot be used. Recalling that it is a parameter that is shared between two functions:

$$\text{Print Resolution} = f(T, \Delta P, d) \qquad (1)$$

$$\Delta P = f(\alpha, d) \qquad (2)$$

By varying *d*, and arbitrarily setting α=120^o a curve fit was done in MATLAB to observe the sensitivity of pressure drop while varying the nozzle diameter (see Appendix A5). It was found that an empirical relationship where *d* varies exponentially with ΔP in equation (2) is characterized by the function:

$$\Delta P = 2.54\ x\ 10^{11} e^{-32.87d}$$

It should also be mentioned that for other values of α, the curve fit function follows a similar pattern; but the rate of change for lower α values was be greater. Essentially, this meant that pressure drop was more abrupt for lower values of α. Furthermore, on a qualitative or intuitive basis, *Print Resolution* varies linearly with *d* in equation (1) since the smaller the *Nozzle exit diameter*, the finer the extruded filament. From the data plotted in Figure 11, it appears that the configuration that represents the lowest pressure drop is *d=0.5mm and* α=120^o. However, this does not imply best overall *Print Resolution* because the *Print Resolution* is also a linear function of *d* in equation 2.

From a quantitative and qualitative standpoint, it is reasonable to suggest that the overall preferred configuration is: *d*=0.3mm and α=120^o. To justify this claim, consider Figure 11; it can be seen that decreasing the nozzle diameter appears to increase the pressure drop exponentially.

Direction of change (↑ ***or*** ↓)	**Change in** ΔP **(↑** ***or*** **↓)**
↓ (from 0.4mm to 0.3mm)	↑ by 6,961 kPa
↓ (from 0.3mm to 0.25mm)	↑ by 55,929 kPa

Table 1 The effect of varying the nozzle exit diameter

To illustrate this relation in an example, Table 1 shows that if *d* was reduced from 0.4mm to 0.3mm, the average pressure drop increased by approximately 6,961 kPa. However, further

reducing d by a smaller interval this time (from 0.3mm to 0.25mm) results in an average pressure drop of 55,929 kPa, which is an entire magnitude greater than the previous case. Therefore, on a CFD basis, the magnitude of the pressure drop is primarily governed by the nozzle diameter. Figure 12 illustrates this effect via a plot of Pressure Drop vs. Nozzle Diameter for the case of d=120^o.

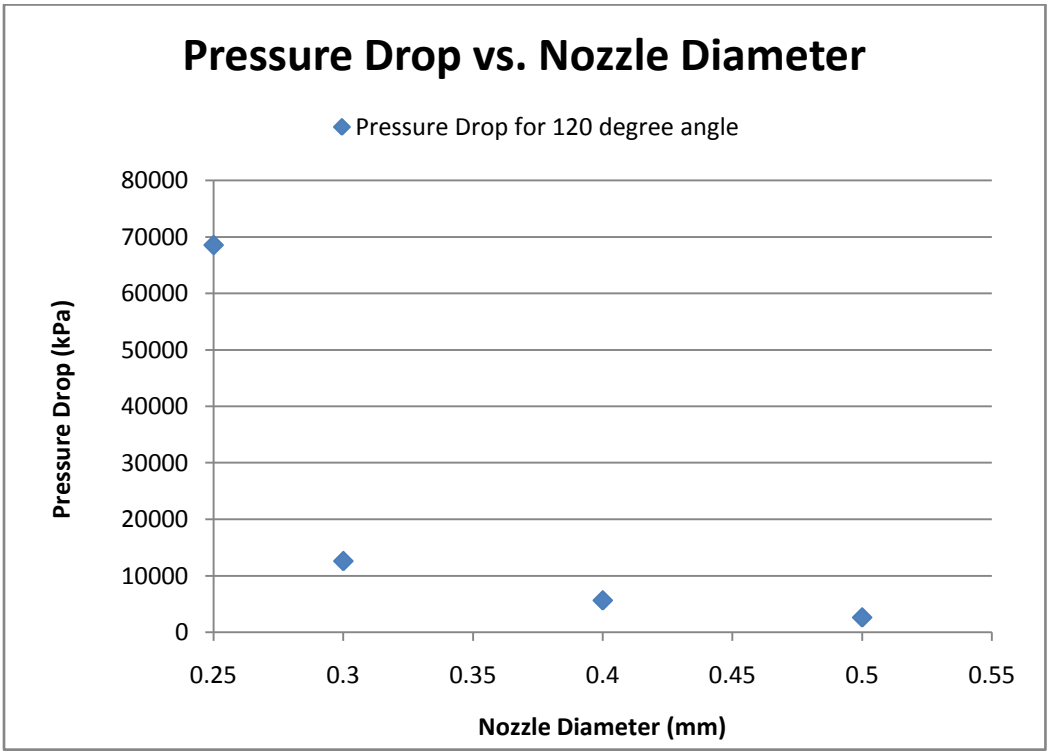

Figure 12 Pressure Drop vs. Nozzle Diameter for d = 120^o

Furthermore, it can be seen that for each of the three plots (each representing a different nozzle diameter), the slope of these lines (or the rate of change) of ΔP increases with increasing d in all cases. But also take note that at lower nozzle diameters, sweeping the nozzle angle from 30^o to 120^o resulted in slightly more abrupt changes in pressure drop than those of higher nozzle diameters. Therefore, at lower nozzle diameters, modifying the nozzle angle will had a more detrimentally sensitive effect on the pressure drop across the liquefier. Based on *Pressure Drop*

alone, one can say that larger nozzle diameters are preferred over the lower ones. However, the challenge was to also minimize the filament diameter (i.e. Nozzle Diameter) for best *Print Resolution* in order to satisfy both equations 1 and 2. Since Figure 11 shows that the smaller the *d*, the higher the ΔP, a cut-off point (optimum) to which one can reduce *d* needed to be found. This optimum falls between the range (0.25mm to 0.4mm). From Figure 11, it is reasonable to suggest (on an intuitive basis) that this cut-off point should be in the vicinity of 0.3mm, since decreasing it further resulted in an abrupt rise in ΔP. Thus, setting d=0.3mm and $\alpha=120^o$ yields ΔP =12637kPa. Even though using a 0.4mm diameter nozzle is an improvement from the original diameter of 0.5mm, setting *d* to 0.3mm provides a greater overall *Print Resolution* with only a small increase in ΔP. Furthermore, seeing from Figure 11 that d=0.25mm corresponded to a ΔP of 68566kPa; not only does this deteriorate the *Print Resolution* by yielding such a high ΔP, but the 23RPM Solarbotics GM3 drive screw motor that the RepRap currently uses can only provide up to $0.423N \cdot m$ of torque on an input voltage of 6VDC, which is insufficient to handle pressure drops of this magnitude. No other gear motor of same size and weight delivers more torque. Therefore, to go any higher would also further increase cost and introduce other trade-offs. The next two sections (3.2.2 and 3.2.3) introduce the final liquefier design and the most feasible gear motor for the RepRap.

3.2.2 The Final Chosen Design Based on CFD Analysis

Initially, it was mentioned that the Print Resolution is a function of both Pressure Drop, and the Nozzle Exit Diameter. Essentially, the purpose was to look at which nozzle diameters and angles would cause the least pressure drop via CFD analysis and to obtain the required compressive force, and hence, the most appropriate torque and RPM the motor needs to provide. This was found in the case of d=0.3mm. On the whole, the most balanced solution is to have

0.3mm diameter nozzle with 120^o nozzle angle. Appendix A3 shows the CFD simulation for the chosen design. The next section calculates the required gear motor settings for this design.

3.2.3 New Motor Torque and RPM Settings for the Final Chosen Design

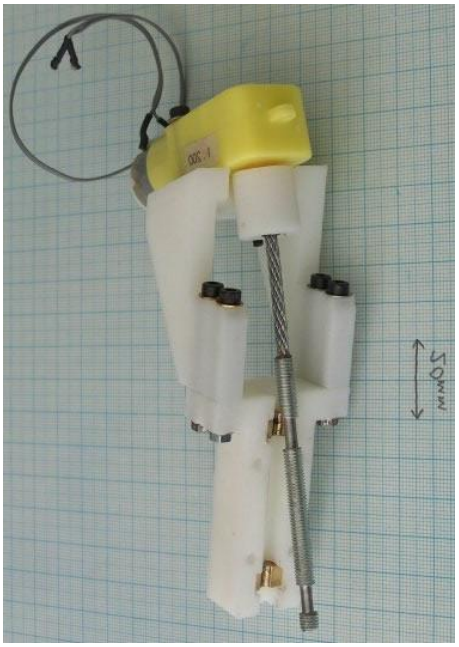

Figure 13 RepRap extruder drive screw
(Image taken from www.reprap.org)

Based on CFD analysis, a more preferable motor RPM setting that corresponded to the revised parameters presented previously in chapter 3.2.1 is calculated as follows:

Using the power screw equation for ACME threads, the torque (T_d) required to drive a load *F*, through in the direction of gravity is given by [13]:

$$T_d = \frac{F d_p}{2} \frac{(\mu \pi d_p - L)}{(\pi d_p + \mu L)}$$

Drive screw specifications:

Pitch diameter (d_p)	6mm
Pitch (L)	1mm
Coefficient of dynamic friction between metal and plastic (μ)	0.3

Table 2 RepRap drive screw specifications

Gear Motor Torque Requirements

Applying the power screw equation to the RepRap drive screw seen in Figure 13, the torque required to push the PCL feedstock downward (T_d) is calculated as:

$$T_d = \frac{(89N)(0.006m)}{2}\frac{[(0.3)(\pi)(0.006m) - (0.001m)]}{[(0.3)(0.006m) + (0.3)(0.001m)]} = 0.592N \cdot m$$

Essentially, this torque corresponds to the pressure drop for the chosen design for the improved configuration where *d*=0.3mm and α=120^o. Comparing this torque to that of the current RepRap motor settings (where $T_{d,current} = 0.423N \cdot m$), it can be said that the most suitable torque specification that will allow for improved *Print Resolution* for the RepRap is approximately $0.592N \cdot m$, which would require an upgrade to a higher performance motor.

Corresponding Gear Motor RPM Specifications

The gear motor power is defined as:

$$P = T_d \omega$$

From www.reprap.org, it was found that the current supplied by the motor is 750mA. Since two AA batteries are required to operate the motor, the motor power for the RepRap is calculated as:

$$P = VI = (3V)(0.75A) = 2.25W$$

The angular velocity is then calculated as:

$$\omega = \frac{P}{T_d} = \frac{2.25W}{0.592N \cdot m} = 3.8\, rad/s$$

Finally, an appropriate RPM setting for the RepRap motor is:

$$RPM = \frac{\omega}{\frac{2\pi}{60}} = \frac{3.8 rad/s}{\frac{2\pi}{60}} = 36.3RPM$$

New Gear Motor for the RepRap

The SilverPak 17C gear motor [23] provides up to $0.599N \cdot m$ of torque, satisfying these new performance requirements. But the trade-offs are that it requires 7VDC input, and also adds additional weight and size. Even though these are compromises, the improved *Print Resolution* of the extruder is of more importance. Thus, it is recommended that the RepRap should upgrade to the SilverPak 17C gear motor.

3.2.4 CFD Model Limitations

The CFD modelling software, COSMOS FloWorks does not provide the ability to model the melt exiting the nozzle of the liquefier. This would be needed to observe the flow behaviour of the melt. Since the CFD model does not demonstrate the evolution of the road in the deposited layer, rheological experiments are needed to show the effect of using a nozzle diameter of 0.3mm on the extruded melt. Furthermore, the CFD simulation in Floworks uses an iterative convergence scheme to arrive at the solution.

The accuracy of the solution rises with the number of iterations selected by the user. Each iteration consumes time, depending on the speed of the processor. For this research, the solution was expected to converge within 40 iterations. Even though theoretically, more iterations should render better results, it was seen that the residuals were negligible when running 40 iterations vs. 100 iterations. For one particular trial iteration, this margin of error was less than 1%. Since each simulation requires an immense amount of time, the CFD analysis was conducted with a more controlled number of iterations, which could have introduced very minor uncertainties.

Overall, it was more accurate to choose the numerical model as a tool for evaluation and selection of the final liquefier design since it carries fewer limitations that results in less severe consequences. The following section justifies this claim.

3.3 Comparison Between CFD and Mathematical Models for Polycaprolactone (PCL)

Figure 14 is essentially a duplication of Figure 8 with the addition of the numerical model (shown in purple). The pressure drop plot is similar to that of the CFD model (shown in red). Figures 15 through 22 show comparison plots between the mathematical and CFD for different nozzle diameters and angles. The CFD model was used as a basis or evaluating the percent error yielded by the mathematical model (shown by vertical bars).

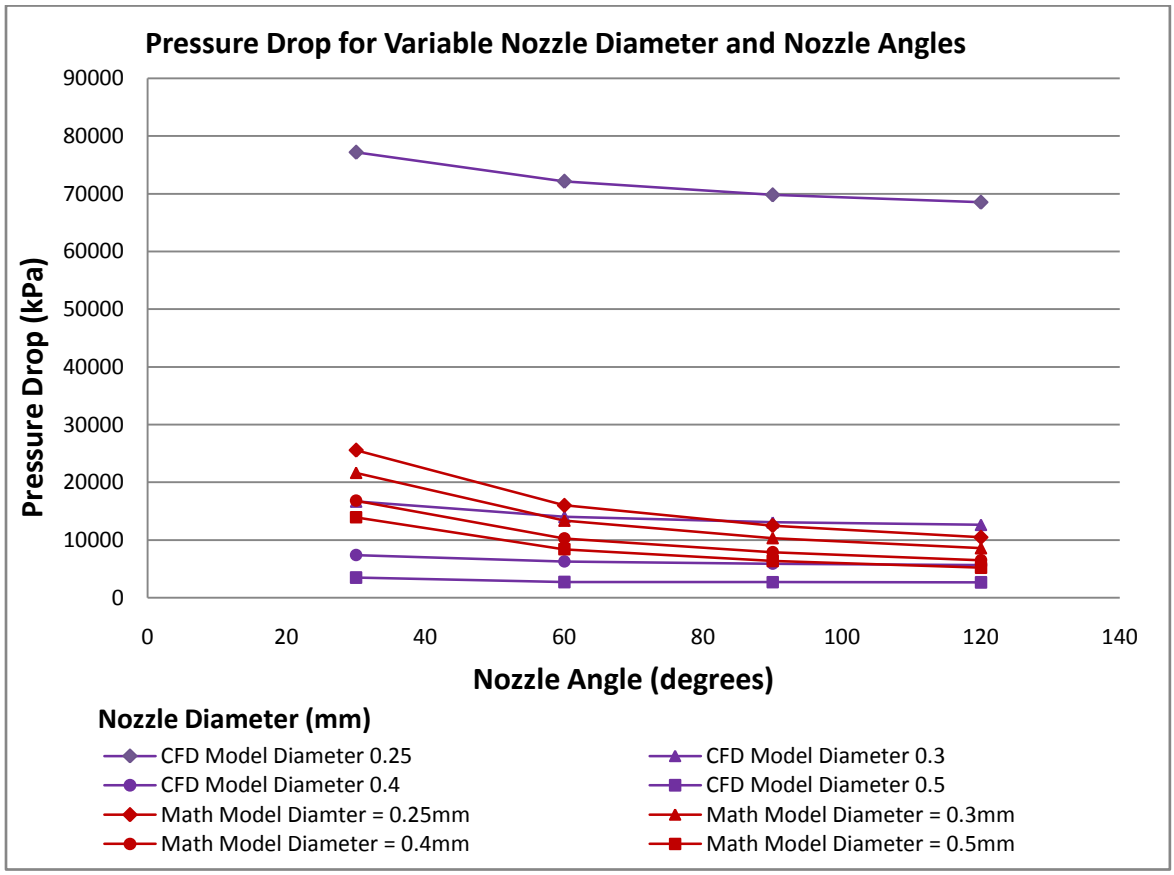

Figure 14 Mathematical Model and CFD Model Comparison: Pressure drop vs. Nozzle Angle

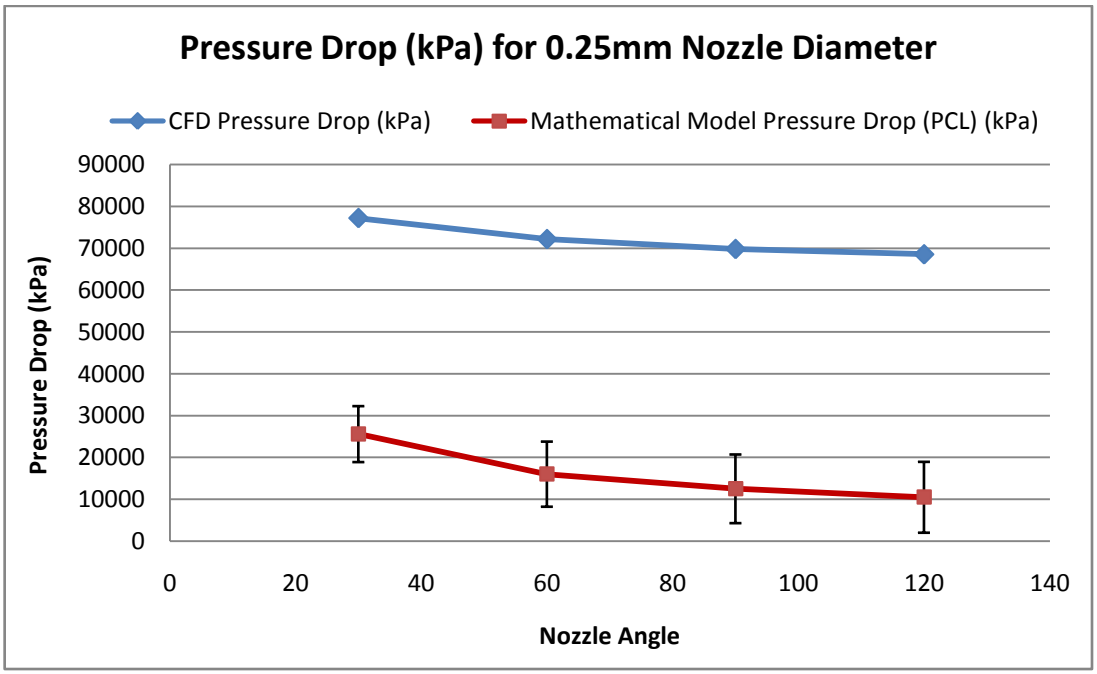

Figure 15 Comparison Between CFD and Mathematical Models for PCL for d=0.25mm

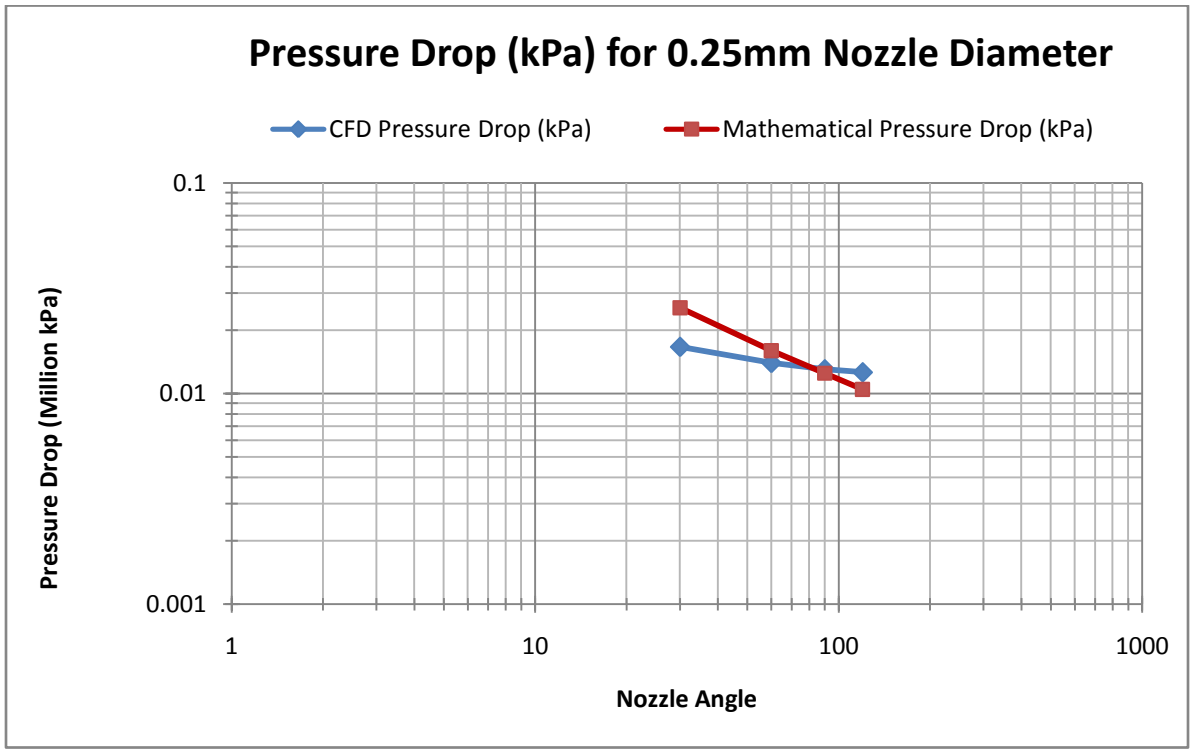

Figure 16 Log Plot Comparison Between CFD and Mathematical Models for PCL for d=0.25mm

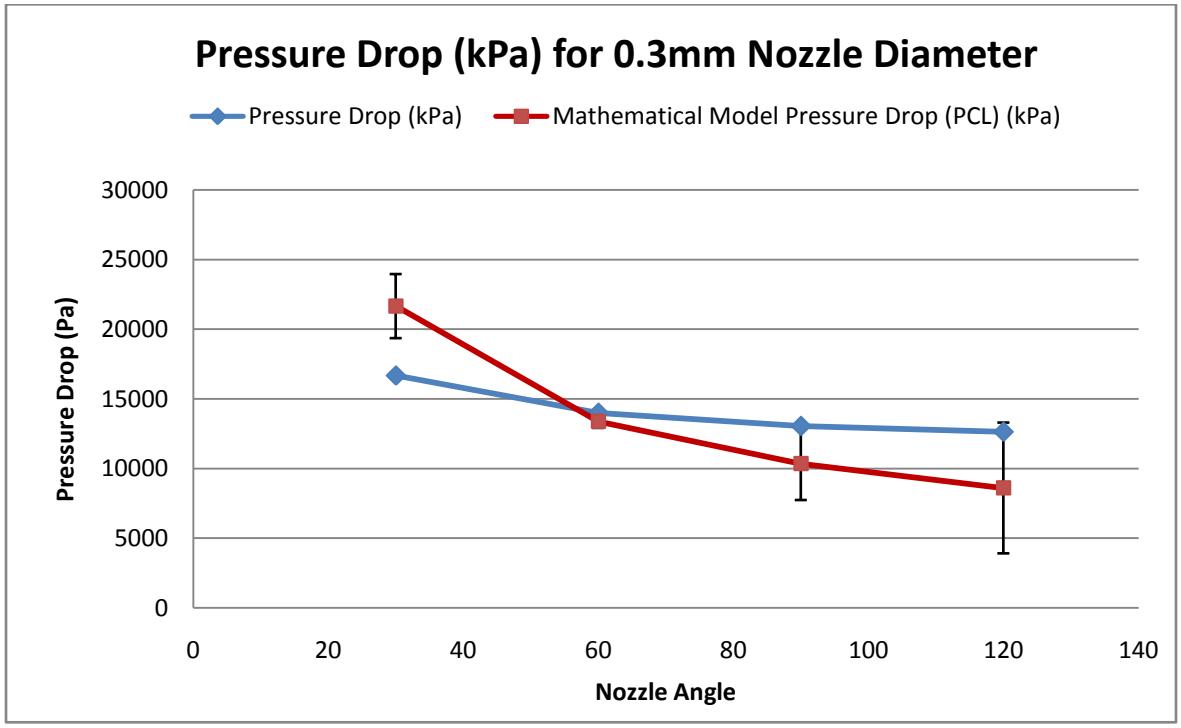

Figure 17 Comparison Between CFD and Mathematical Models for PCL for d=0.3mm

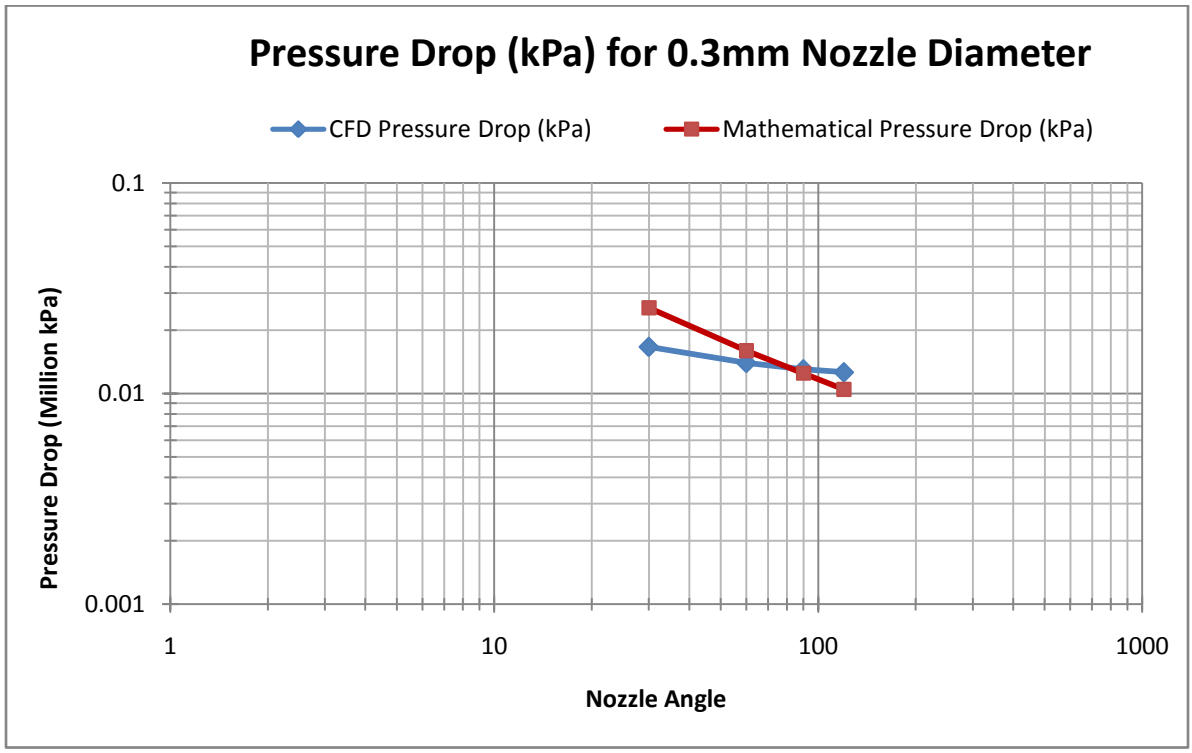

Figure 18 Log Plot Comparison Between CFD and Mathematical Models for PCL for d=0.3mm

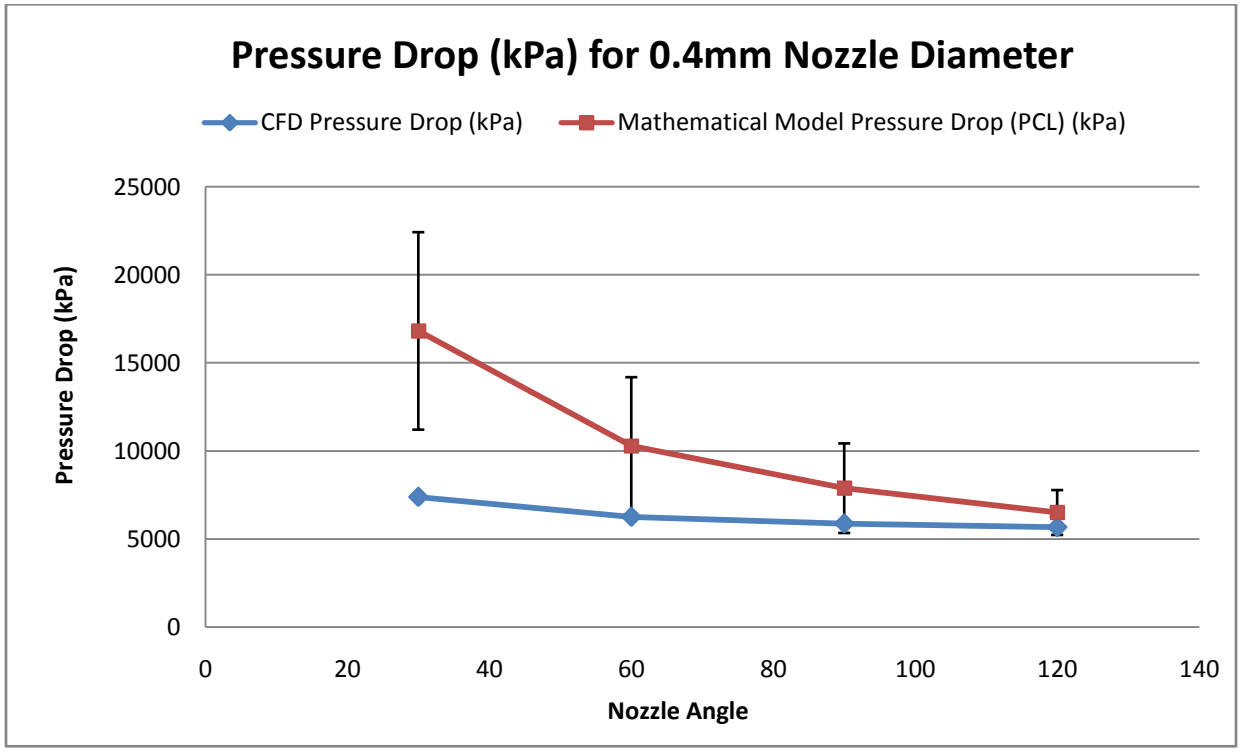

Figure 19 Comparison Between CFD and Mathematical Models for PCL for d=0.3mm

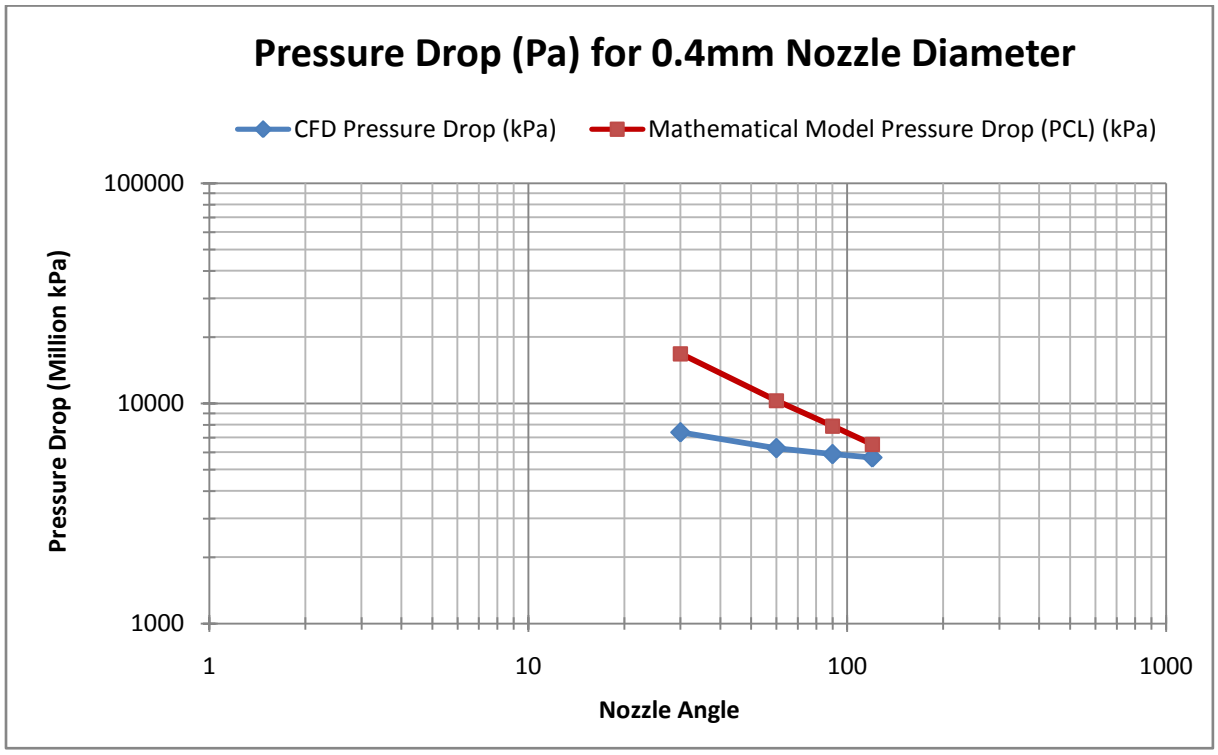

Figure 20 Log Plot Comparison Between CFD and Mathematical Models for PCL for d=0.3mm

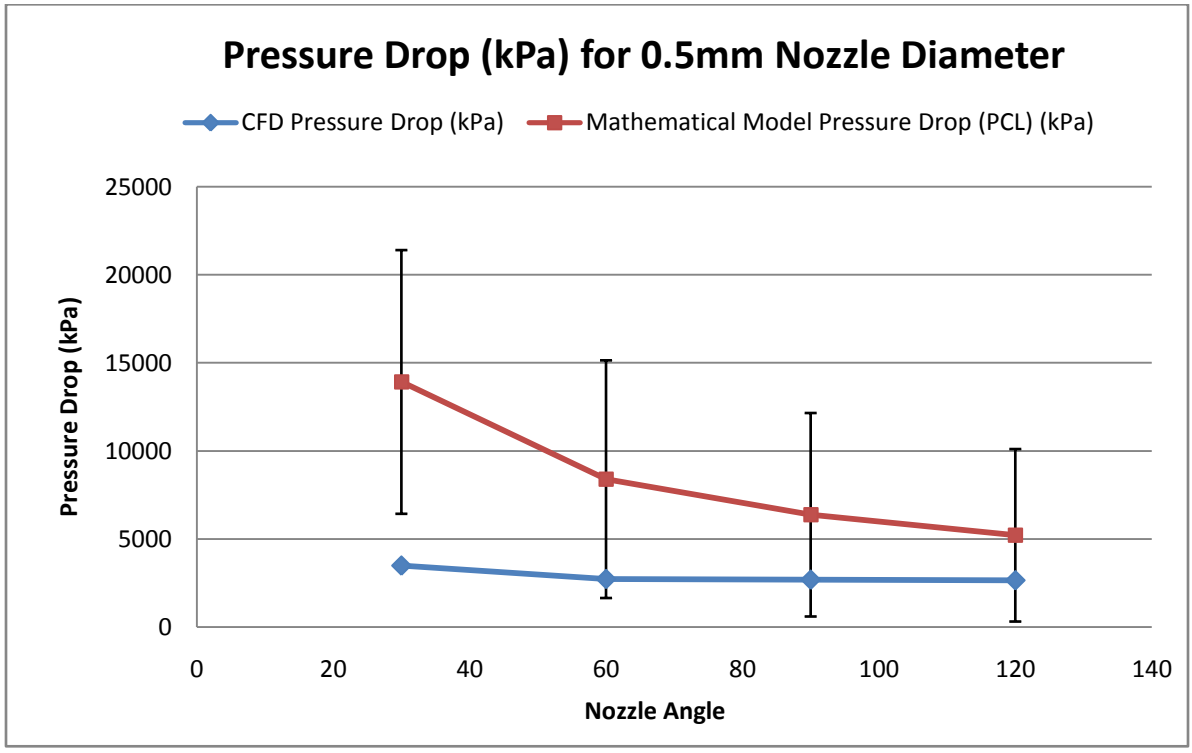

Figure 21 Comparison Between CFD and Mathematical Models for PCL for d=0.3mm

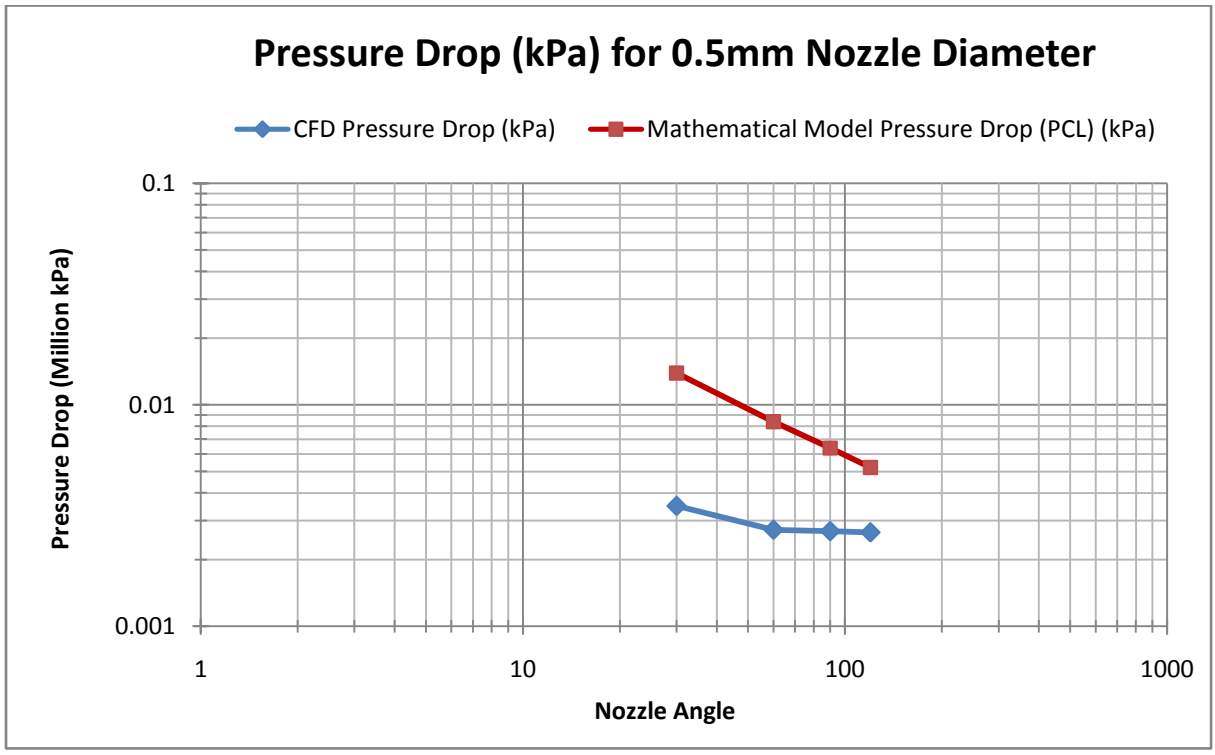

Figure 22 Log Plot Comparison Between CFD and Mathematical Models for PCL for d=0.3mm

Recalling that from the sensitivity analysis for the theoretical model earlier in chapter 3.1.2, drastic differences in pressure drops resulted when the material index constant was modified; the lower the d, the more abrupt the change in ΔP. This is also reflected in the plots shown in Figures 15 to 22. To view this order of magnitude change more clearly, logarithmic *Pressure Drop vs. Nozzle Angle* plots were also presented. The theoretical models (red lines) have higher rates of change in ΔP (i.e. higher slopes) as nozzle angle changes. This was attributed to the fact that the theoretical model displays higher sensitivity to changes in material index (m). To further verify this, an equivalent sensitivity analysis was conducted for the numerical model (although not shown here). It was found that increasing the material index exhibited negligible changes in *Pressure Drop* for all *Nozzle Angle* values. Hence, this justifies

the "flatter" shape of the logarithmic plots of the numerical (CFD) models (blue lines) in comparison with those of the theoretical.

Other than the mathematical model's errors due to the sensitivity of the results caused by changes in the material and fluid indices, there were other sources of error that contributed to the difference in results. Viscosity data used in the CFD simulation was provided directly from the manufacturer of the particular PCL material used in the RepRap. The value of viscosity used was 8000 Pa-s at 100°C and a zero shear rate. Realistically, the shear rate is above zero and the temperature is not at 100°C and both of these factors affect the true value of viscosity. Since viscous forces dominate over inertial forces in this type of flow, an inaccurate value of viscosity can change the resulting pressure drop. Figures 15 through 22 show the relative error bars. On average, the percentage error generated by the theoretical model for *Pressure Drop* was approximately 34%.

Another important limitation to using the mathematical model was that it inaccurately assumes isothermal conditions throughout the entire length of the liquefier while the CFD model did not since the temperature of the feedstock entering the liquefier did not instantly change to the inner wall temperature of 330K. The entrance length required to achieve this steady state isothermal condition was approximately 17mm. This CFD temperature profile is shown in Appendix A2.

4.0 Laboratory Fluid Analysis with Polycaprolactone

The purpose of the experimental analysis was to gather data on the melt flow behaviour as it exits the extruder. The Numerical and Theoretical studies both used an inlet velocity of 0.0011 m/s. There, the experiment operated using a flow velocity as close as possible to 0.001 m/s because it was important to observe how the exit melt flow deforms as a result of what

happened inside the liquefier from the previous numerical study, thus the experiment provides another picture of how print resolution is affected by swelling and shrinking effects.

In order to better determine the validity of Polycaprolactone to the RepRap application, a laboratory experiment was conducted using the apparatus in Appendix A6. For PCL, the temperature of the liquefier flow channel should be adjusted to slightly above the melting temperature (i.e. slightly above 330K). Also, the motor used in the experiment was a Solarbotics GM3, with a peak torque of $0.299N \cdot m$ (though this was not the newly recommended model discussed in chapter 3.2.3). The diameter of the filament at the liquefier exit was measured upon exit and after solidification. The following characteristics were evaluated to justify the filament quality:

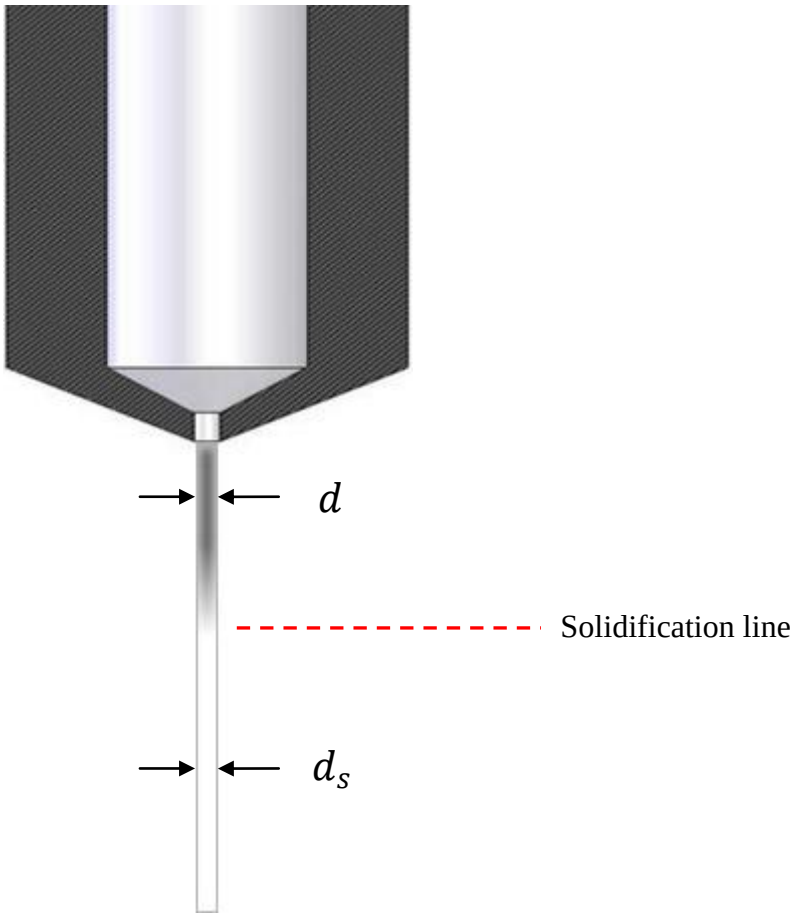

Figure 23 Filament diameter at liquefier exit (see Appendix A6 for actual experiment)

Mean filament diameter at liquefier exit (d)

Using a high precision camera, a measurement of the exit diameter was taken on a periodic basis. The mean diameter at liquefier exit was calculated to represent the average precision of the filament

Mean filament diameter after solidification (d_s)

This took the same approach as in the previous.

Shrinkage factor

This was found by performing the calculation: d_s/d. The higher the shrinkage factor, the lower the dimensional accuracy and consistency of the printed part (see Figure 23).

Fluid behaviour upon exit

The characteristics of the polymer as it exits the liquefier was observed

Distance to solidification

This is the vertical downward distance from the nozzle liquefier exit the point where the PCL filament becomes fully solidified (see Figure 23).

All of the above mentioned characteristics are recorded in Table 3.

4.1 Results of PCL Laboratory Fluid Analysis

	Trial 1	Trial 2	Trial 3
Velocity	0.00067m/s	0.00072m/s	0.00078m/s
Distance to solidification	25.5mm	30.5mm	40mm
Reynolds Number	< 1	< 1	< 1
Mean filament diameter at liquefier exit (*d*)	0.6mm	0.7mm	0.7mm
Mean filament diameter after solidification (d_s)	0.6mm	0.7mm	0.7mm
Shrinkage Factor (d_s/d)	1.14	1	1
Mean caliper reading of filament diameter	0.59mm	0.64mm	0.66mm
Die Swell Ratio	1.18	1.28	1.32

Table 3 Polycaprolactone (PCL) Laboratory Fluids Analysis Results

A total of three trials were completed and tabulated in Table 3. They were conducted in an order such that the filament feed speed was slightly greater each time. The experiment was captured on video using a 35X optical zoom video camera, and analyzed in depth (see Appendix A6). The filament velocity was calculated by the formula $V = \frac{\Delta d}{\Delta t} = \frac{\Delta d}{10mm}$ simply by observing the time required for a single particle on the filament to travel a displacement of 10mm. Static images were extracted from the videos and imported into the Macromedia Fireworks imaging software for further analysis. In order to view the approximate dividing boundary between liquid and fully solidified PCL filament with greater clarity, an image filter was applied to increase the contrast. From this, the "Distance to solidification", "Mean filament diameter at liquefier exit (d)", and "Mean filament diameter after solidification (d_s)" were obtained and are shown in Table 3.

From the data collected, it can be noted that the distance required for solidification decreases for lower velocity readings, which is also intuitive since the lower the extrusion rate, the more time is allotted for cooling at earlier stages.

4.2 The Die Swell Effect

Fluids that converge and extrude out of the circular nozzle orifice typically do not have the same diameter as the nozzle exit diameter. There is a tendency to swell upon exit. The die swell ratio which compares the melt diameter to the nozzle diameter indicates how much expansion the extruded melt undergoes as it exits the nozzle. It was observed that an increase in velocity resulted in increasing die swell. The diameter of the fully solidified extruded melt was measured with a digital calliper, accurate to the nearest 0.01mm (note: each measurement was an average of several points along the solidified section of the extruded melt), and recorded in

Table 3. The calliper reading for trial 1 was measured to be 0.59mm, which is greater than trials 2 and 3 (0.64mm and 0.66mm respectively). This is because trials 2 and 3 are of higher velocities. In order to increase velocity, the force and pressure required to push the filament at the liquefier entrance must also be greater. This generates a larger pressure drop (ΔP) across the liquefier, which in turn degrades the filament resolution, causing it to expand (recalling from earlier that the print resolution is a function of ΔP). An explanation of this phenomenon rises from the fact that polymers such as PCL have viscoelastic properties. The melt undergoes two deformations, one due to the convergent section of the channel and the second due to the shear caused by changes in the velocity profile within the channel. These deformations are stored elastically and the swelling effect is caused by the release of the elastic deformation of the extrudate [12]. The die swell ratios range from 1.18 to 1.32 which fall into agreement with die swell ratios of common high molecular weight polymeric fluids at low Reynold's numbers [3].

From the shrinkage factor readings, it can also be confirmed that the fluid used is shrink-resistant, as expected since the ratio of the filament diameters before and after solidification remained the same for all three trials. This is ideal because any shrinkage during solidification can cause the material layer to be distorted, ultimately resulting in part defects.

The behaviour of the PCL filament at liquefier exit was uniform since it did not display any random behaviour. This is because the high viscosity of PCL generated higher resistance to shear, keeping the fluid intact. The low Reynolds number having a value of less than one indicate this is creeping flow, therefore, inertial effects are negligible and viscous forces dominate.

Overall, swelling effects did play a role in the change of the melt diameter and ultimately, the print resolution, but in the case of the 0.5mm diameter nozzle, the effects were small, keeping the extruded melt as close as possible to the exit diameter.

5.0 Conclusion

There was some confidence in the theoretical model to approximate the pressure drop across the extruder. However, it and the numerical model are not without its limitations. Each case for the numerical (CFD) analysis was performed with forty iterations to save on computational time. The mathematical model is sensitive to changes in the material parameters. Therefore, it was found that there were differences in comparing the pressure drop values. The material parameters φ and m have the greatest influence on the flow behaviour. It has been observed that the effect of varying m is more evident than φ since m is an exponent value whereas φ is a constant of proportionality.

From the results obtained, the design of the RepRap extruder can accommodate a decrease in the nozzle diameter while utilizing the same material, PCL without adverse effects. The proposed redesign suggests the decrease to 0.3 mm nozzle diameter. A study on 0.25 mm diameter revealed that the pressure drop was too large for a reasonable cost motor to be able to accommodate the necessary force required to push the filament through the liquefier.

This study was a simplified case where the fluid stream is steady and continuous which would be ideal if the actual operation of the device created one long unbroken material road layer. In practical operation, the flow is non-continuous and unsteady because there are breaks between each layer and material road where the Cartesian gantry robot requires reposition of the deposition tool head and during those times, no PCL melt is extruded. Additionally, formation of a material road built on top of preceding layers will subsequently cause a change in the road's dimensions. A new model that explores these non-simplified cases should be developed for further study.

The analysis presented in this study focused mainly on numerical methods. The theoretical model had simplifications that could have adverse effects. Therefore, there was more confidence in using the numerical (CFD model). Any further research should continue with numerical methods unless a more stable and conservative theoretical model can be developed to better depict the problem.

Further experimental study is required to observe the exit melt flow utilizing a 0.3mm diameter nozzle as a suggested improvement from numerical studies. Additionally, due to small die swell ratios that occurred at a velocity of 0.0011 m/s, it is worth investigating the change in die swell as a result of increasing velocity. Therefore, the inlet velocity of the melt is another area of study to further improve printing speeds.

Appendices

Appendix A1: Problems with the Original RepRap Liquefier

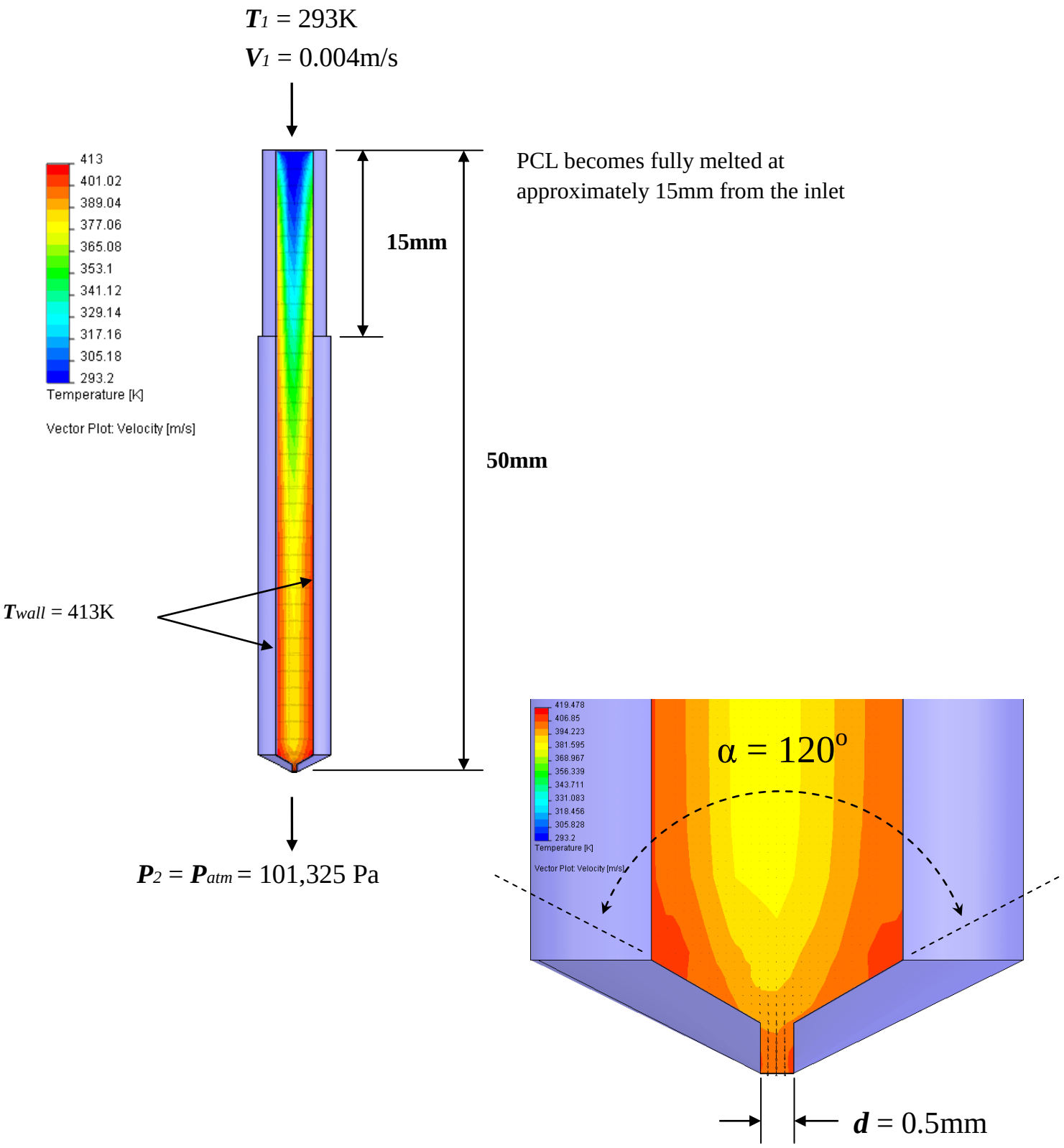

Appendix A2: Improved liquefier configuration based on findings by Bellini [2]

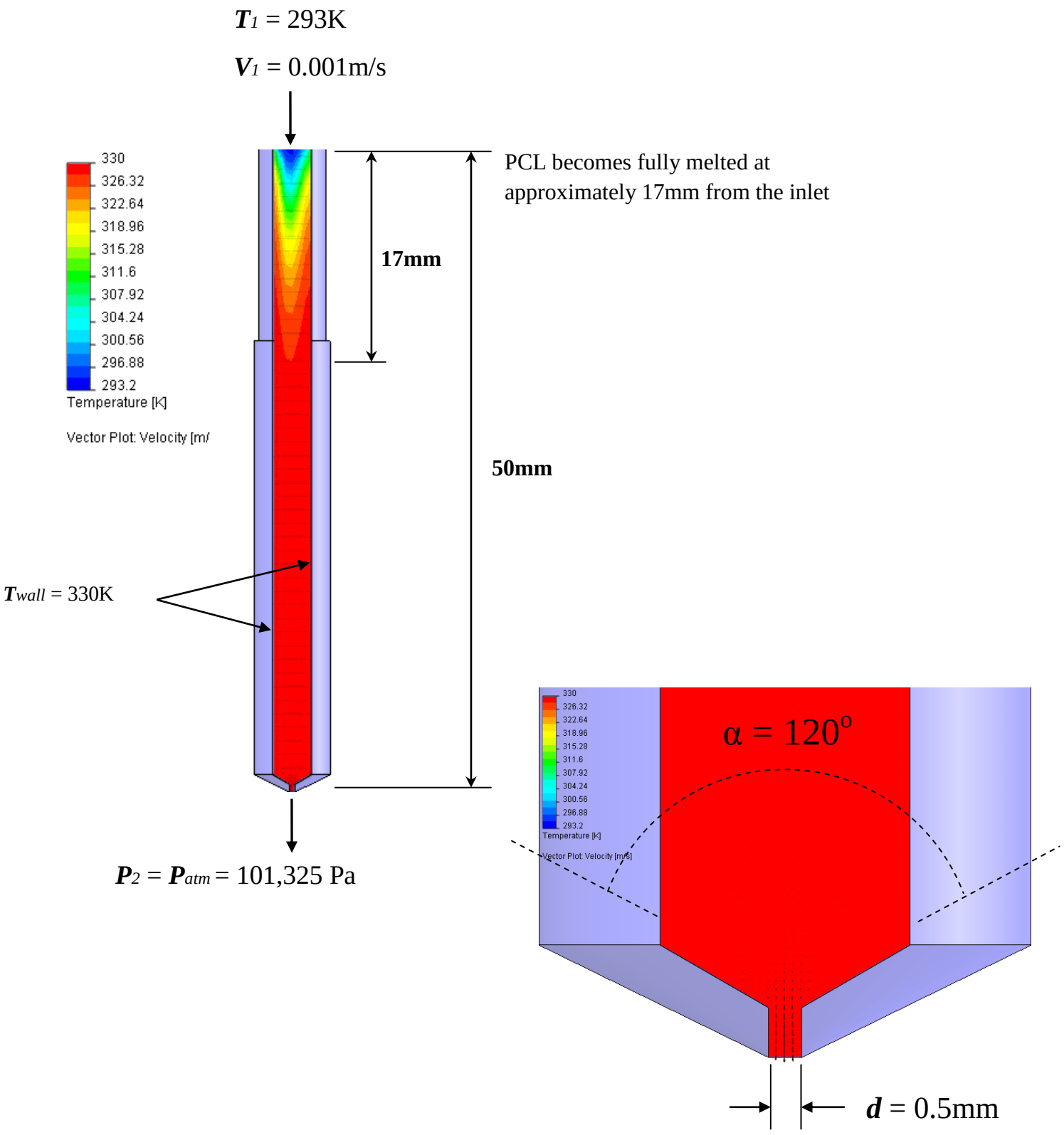

Appendix A3: The final chosen design configuration based on CFD modeling

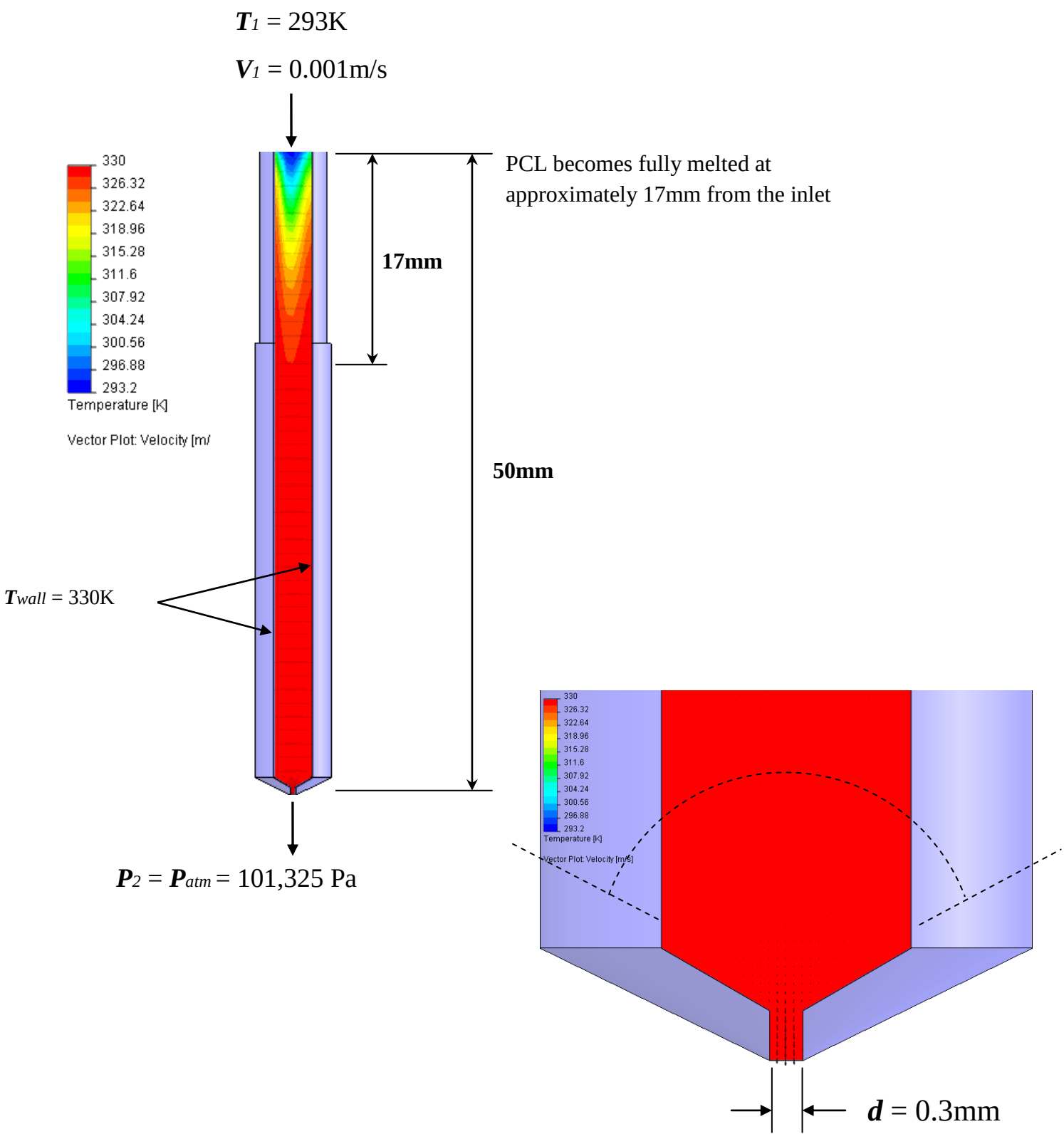

Appendix A4: Apparatus for laboratory fluid analysis

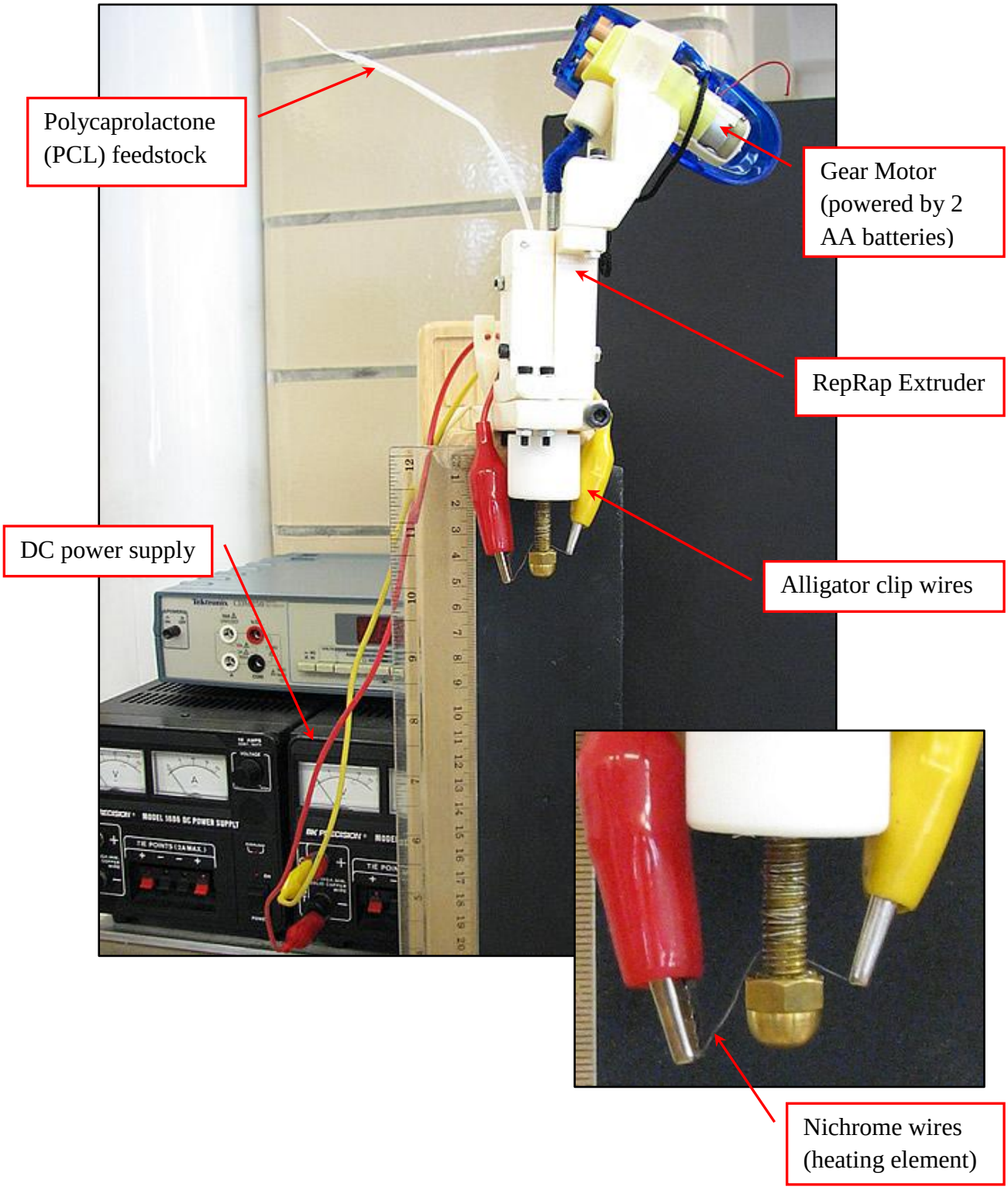

Appendix A5: Sensitivity Analysis Curve Fit for $\alpha = 120^{o}$

**Note: the MATLAB code below represents a sample exponential curve fit, conducted for the scenario in which $\alpha=120^{o}$ angle PCL only. Other values of α will generate similar curves, but are not shown here.

```
General model Exp1:
       f(x) = a*exp(b*x)
Coefficients (with 95% confidence bounds):
       a =   2.54e+011  (-1.486e+012, 1.994e+012)
       b =      -32.87  (-60.06, -5.684)

Goodness of fit:
  SSE: 3.415e+013
  R-square: 0.9882
  Adjusted R-square: 0.9823
  RMSE: 4.132e+006
```

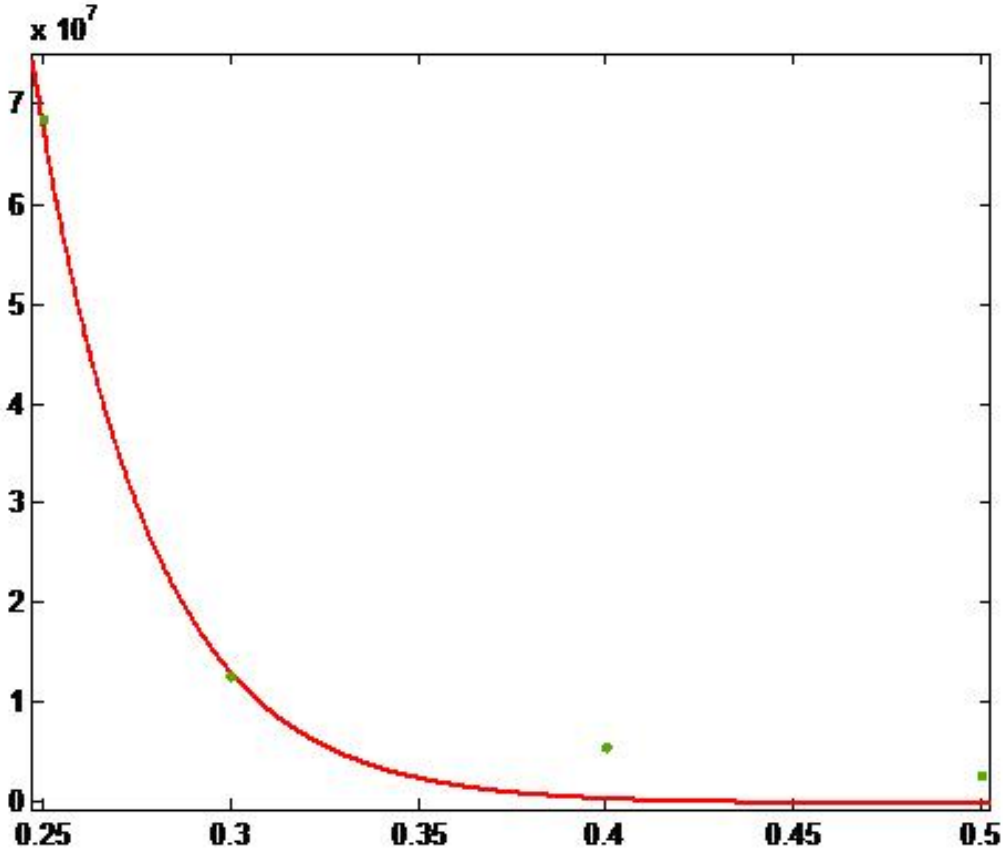

Appendix A6: Polycaprolactone (PCL) Laboratory Fluids Analysis

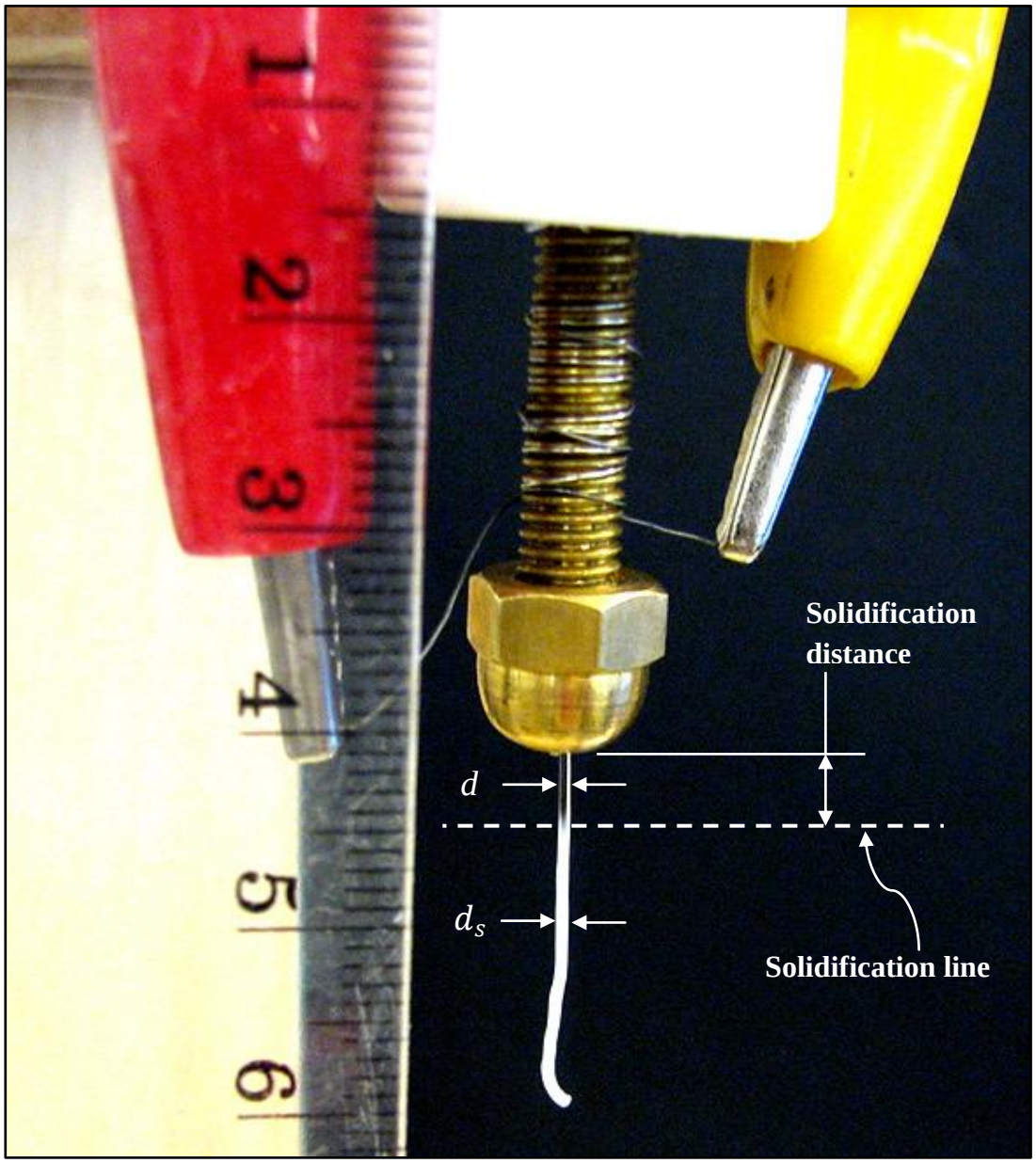

References

[1] Agarwala, M. K., et al. "Structural Quality of Parts Processed by Fused Deposition." Rapid Prototyping Journal 2.4 (1996): 4-19.

[2] Bellini, A. "Fused Deposition of Ceramics: A Comprehensive Experimental, Analytical and Computational Study of Material Behavior, Fabrication Process and Equipment Design." (2002).

[3] Bird, B. R. R., et al. "Dynamics of Polymeric Liquids Volume 2: Kinetic Theory." Dynamics 34 (1988): 1052.

[4] Bowyer, A. "RepRap." online document],[cited. www.reprap.org] (2006).

[5] Crawford, RH, and JJ Beaman. "Solid Freeform Fabrication." Spectrum, IEEE 36.2 (1999): 34-43.

[6] De Waele, A. "Oil Color Chem." Assoc.J 6 (1923): 33.

[7] Grosvenor, MP, and JN Staniforth. "The Effect of Molecular Weight on the Rheological and Tensile Properties of Poly (ϵ-Caprolactone)." International journal of pharmaceutics 135.1-2 (1996): 103-9.

[8] Jenkins, MJ, and KL Harrison. "The Effect of Molecular Weight on the Crystallization Kinetics of Polycaprolactone." Polymers for Advanced Technologies 17.6 (2006): 474.

[9] Kai, C. C. "Three-Dimensional Rapid Prototyping Technologies and Keydevelopment Areas." Computing & Control Engineering Journal 5.4 (1994): 200-6.

[10] Kalambur, S., and S. S. H. Rizvi. "Rheological Behavior of Starch–Polycaprolactone (PCL) Nanocomposite Melts Synthesized by Reactive Extrusion." ENG.SCI 46 (2006): 650-8.

[11] Malone, E., and H. Lipson. "Fab@ Home: The Personal Desktop Fabricator Kit." Rapid Prototyping Journal 13.4 (2007): 245-55.

[12] Michaeli, W. Extrusion Dies for Plastics and Rubber: Design and Engineering Computation—Second Edition, Hanser ed., New York (1992).

[13] Norton, R. L. Machine Design: An Integrated Approach. Prentice Hall, 2000.

[14] Ostwald, W. "Ueber Die Geschwindigkeitsfunktion Der Viskosität Disperser Systeme. II." Colloid & Polymer Science 36.3 (1925): 157-67.

[15] Pham, DT, and RS Gault. "A Comparison of Rapid Prototyping Technologies." International Journal of Machine Tools and Manufacture 38.10-11 (1998): 1257-87.

[16] Ramanath, HS, et al. "Modeling of Extrusion Behavior of Biopolymer and Composites in Fused Deposition Modeling."

[17] Ramanath, H. S., et al. "Melt Flow Behaviour of Poly-Epsilon-Caprolactone in Fused Deposition Modelling." Journal of Materials Science: Materials in Medicine (2007).

[18] Schwach, E., and L. Averous. "Starch-Based Biodegradable Blends: Morphology and Interface Properties." Polymer International 53.12 (2004): 2115-24.

[19] Skoglund, P., and A. Fransson. "Continuous Cooling and Isothermal Crystallization of Polycaprolactone." Journal of Applied Polymer Science 61.13 (1996): 2455-65.

[20] Solvay. MSDS of CAPA 6800 PolyCaprolactone.

[21] Stampfl, J., and R. Liska. "New Materials for Rapid Prototyping Applications." Macromolecular chemistry and physics(Print) 206.13 (2005): 1253-6.

[22] Upcraft, S., and R. Fletcher. "The Rapid Prototyping Technologies." Assembly Automation 23.4 (2003): 318-30.

[23] 1inchengineering.com. (2006). Integrated Motor Controller / Silverpak17C. <www.linengineering.com/site/products/silverpakC.html> .

Responsibilities of Each Group Member

Both group members contributed to all responsibilities. The major contribution by each member is highlighted below.

Stephen Ju

1. Methodology
2. CFD Model Development and Simulation Analysis
3. Experiment Testing, Results Analysis

Mark Roxas

1. Literature Review
2. Theoretical/Mathematical Model Development, Analysis
3. Experiment Physical Construction, Results Analysis

Breakdown of Written Chapters

Both members contributed to each section written. This last best portrays the major contributor to each section

1.0 Introduction - M.R.
2.0 Methodology – S.J.
2.1 Current Problems with the Original RepRap Machine – S.J.
3.0 Improving Boundary Conditions for the Liquefier - S.J.
3.1 Using the Mathematical Model - M.R.
3.1.1 Mathematical Model Results - M.R.
3.1.2 Mathematical Model Sensitivity Analysis – M.R.
3.1.3 Mathematical Model Limitations - M.R.
3.2 The Equivalent Numerical Analysis (CFD Model) – S.J.
3.2.1 Obtaining an Improved d and α Combination S.J.
3.2.2 The Final Chosen Design Based on CFD Analysis S.J.
3.2.3 New Motor Torque and RPM Settings for the Final Chosen Design S.J.
3.2.4 CFD Model Limitations S.J.
3.3 Comparison Between CFD and Mathematical Models for Polycaprolactone (PCL) M.R. & S.J.
4.0 Laboratory Fluid Analysis with Polycaprolactone M.R.
4.1 Results of PCL Laboratory Fluid Analysis M.R.
4.2 The Die Swell Effect - M.R.